Determining reliable histories of slip on normal faults with bedrock scarps using cosmogenic exposure data

H J Goodall[1], Laura Gregory[1], L N J Wedmore[2], K J W Mccaffrey[3], R M J Amey[1], G P Roberts[4], R P Shanks[5], R J Phillips[1], and A Hooper[1]

[1]University of Leeds
[2]University of Bristol
[3]Durham University
[4]Birkbeck, University of London
[5]SUERC, University of Glasgow

November 28, 2022

Abstract

Cosmogenic exposure data can be used to calculate time-varying fault slip rates on normal faults with exposed bedrock scarps. However, the method relies on assumptions related to how the scarp is preserved, which should be consistent at multiple locations along the same fault. Previous work commonly relied on cosmogenic data from a single sample locality to determine the slip rate of a fault. Here we show that by applying strict sampling criteria and using geologically informed modelling parameters in a Bayesian-inference Markov chain Monte Carlo method, similar patterns of slip rate changes can be modelled at multiple sites on the same fault. Consequently, cosmogenic data can be used to resolve along-strike fault activity. We present cosmogenic 36Cl concentrations from seven sites on two faults in the Italian Apennines. The average slip rate varies between sites on the Campo Felice Fault (0.84 0.23 to 1.61 0.27 mm yr ˆ-1), and all sites experienced a period of higher than average slip rate between 0.5 and 2 ky and a period of lower than average slip rate before 3 ky. On the Roccapreturo fault, slip rate in the centre of the fault is 0.550.11 and 0.350.05 mm yr ˆ-1 at the fault tip near a relay. The estimated time since the last earthquake is the same at each site along the same fault. These results highlight the potential for cosmogenic exposure data to reveal the detailed millennial history of earthquake slip on active normal faults.

Determining reliable histories of slip on normal faults with bedrock scarps using cosmogenic exposure data

H. J. Goodall[1], L. C. Gregory[1], L. N. J. Wedmore[2], K. J. W. McCaffrey[3], R. M. J. Amey[1], G. P. Roberts[4], R. P. Shanks[5], R. J. Phillips[1*], A. Hooper[1]

[1]COMET, School of Earth and Environment, University of Leeds, UK
[2]Department of Earth Sciences, University of Bristol, Bristol, UK
[3]Department of Earth Sciences, Durham University, Durham, UK
[4]Department of Earth and Planetary Sciences, Birkbeck, University of London, UK
[5]Scottish Universities Environmental Research Centre (SUERC), East Kilbride, UK

Key Points:

- Fault slip rates constrained with cosmogenic isotopes from multiple sites on the same fault agree.
- Fault slip rate varies during the Holocene, and pulses of rapid slip rate are temporally correlated along strike.
- Cosmogenic isotopes on bedrock fault scarps provide a detailed record of activity, provided the sample locations are carefully selected.

[*]Current address, Edinburgh

Corresponding author: Laura C. Gregory, `l.c.gregory@leeds.ac.uk`

Abstract

Cosmogenic exposure data can be used to calculate time-varying fault slip rates on normal faults with exposed bedrock scarps. However, the method relies on assumptions related to how the scarp is preserved, which should be consistent at multiple locations along the same fault. Previous work commonly relied on cosmogenic data from a single sample locality to determine the slip rate of a fault. Here we show that by applying strict sampling criteria and using geologically informed modelling parameters in a Bayesian-inference Markov chain Monte Carlo method, similar patterns of slip rate changes can be modelled at multiple sites on the same fault. Consequently, cosmogenic data can be used to resolve along-strike fault activity. We present cosmogenic ^{36}Cl concentrations from seven sites on two faults in the Italian Apennines. The average slip rate varies between sites on the Campo Felice Fault (0.84 ± 0.23 to 1.61 ± 0.27 mm yr $^{-1}$), and all sites experienced a period of higher than average slip rate between 0.5 and 2 ky and a period of lower than average slip rate before 3 ky. On the Roccapreturo fault, slip rate in the centre of the fault is 0.55 ± 0.11 and 0.35 ± 0.05 mm yr $^{-1}$ at the fault tip near a relay. The estimated time since the last earthquake is the same at each site along the same fault. These results highlight the potential for cosmogenic exposure data to reveal the detailed millennial history of earthquake slip on active normal faults.

1 Introduction

Fault activity constrained over multiple earthquake cycles and across fault systems helps to address fundamental questions of how faults interact (Nixon et al., 2016; Wedmore et al., 2017; Cowie et al., 2017; Mueller, 2017), how tectonic strain accumulates and is released on brittle faults (Hergert & Heibach, 2010; Ferry et al., 2011), and how fault slip varies in time and space (Nicol et al., 2010; Dolan et al., 2016). Fault slip rates can be measured or inferred using a variety of tools, including geodesy (Bendick et al., 2000; Walters et al., 2013; Hussain et al., 2016), palaeoseismology and historical records (Pantosti et al., 1996; Galli et al., 2008; Cinti et al., 2019), and dating of offset geological, geomorphological, and man-made features (Phillips et al., 2004; Zechar & Frankel, 2009; Wang et al., 2011; Gregory et al., 2014; R. D. Gold et al., 2017; Mechernich et al., 2018). Each method has different spatial and temporal coverage and resolution, and as a whole provide insight into tectonic processes occurring over a range of scales. Despite the range of techniques, there are still discrepancies between long-term average slip rates and geodetic strain rates, which in part may be due to methodological uncertainties and problems related to the preservation of earthquake surface deformation in the geological or geomorphological record (R. D. Gold et al., 2009; Schmidt et al., 2011; Searle et al., 2011). Individual earthquakes often have incomplete or variable surface displacements along strike (and at depth; Bull et al., 2006; Wesnousky, 2008; Rockwell & Klinger, 2013; P. O. Gold et al., 2013; Ando et al., 2017; Walters et al., 2018), and if patterns of variable displacement persist over multiple earthquake cycles, cumulative Quaternary displacement and slip rate will be different along the fault.

By sampling multiple locations along a single fault, it is possible to test the influence of along-strike variation in earthquake slip and preservation on Quaternary slip rate. Bedrock normal fault scarps are excellent targets for investigating along-strike slip variation because they record a more temporally detailed history of progressive fault exposure compared to displaced landforms (Benedetti et al., 2002; Schlagenhauf et al., 2010; Akçar et al., 2012; Cowie et al., 2017; Mechernich et al., 2018). In the Mediterranean, scarps in limestone have been preserved since the Last Glacial Maximum (LGM; Armijo et al., 1992; Giraudi, 1995; Tucker et al., 2011), accruing slip over multiple earthquake cycles. The rate of exhumation of the fault plane by earthquakes can be determined with measurements of the cosmogenic isotope chlorine-36 (^{36}Cl), which primarily accumulates in the scarp as a result of progressive exposure to cosmic radiation and production from abundant calcium (Ca) present in the limestone footwall (Gosse & Phillips, 2001). A forward model is required to determined fault slip rates and the pattern of exhumation through time. Normal fault scarps have a complex exposure history that starts to develop when the fault is buried several metres below the surface, and the same profile of ^{36}Cl can result from different earthquake time and displacement histories as a result of partial exposure to cosmic radiation whilst buried. Though many previous studies suggest that the timing of individual earthquakes can be determined by this technique (Benedetti et al., 2002; Schlagenhauf et al., 2010; Akçar et al., 2012; Benedetti et al., 2013; Tesson et al., 2016; Tesson & Benedetti, 2019), our primary aim is to determine fault slip rates and slip rate variations.

Cumulative fault slip can vary along strike on an individual fault as a result of (1) the natural along-strike displacement profile (Cowie & Shipton, 1998); (2) complexity of fault structure such as overlapping segments (Peacock & Sanderson, 1991); or (3) due to problems in the long-term preservation of displacement as a result of slope instability. In the case of (1) or (2), we would expect the total displacement to vary at different localities, but the timing of major slip rate changes should be temporally correlated along-strike if earthquakes typically rupture the length of the fault. Only one study has attempted to document the synchronicity of along-strike fault slip using cosmogenic isotopes on bedrock fault scarps (Schlagenhauf et al., 2011). They were able to model the data from multiple sites with a similar earthquake history, but only by changing the total amount of time that the scarp had been partially exposed at each site by several thousand years (2.5 ka vs 13.0 ka, termed 'pre-exposure'). If this parameter is kept constant between the sites, the data from different sites cannot be modelled with a temporally correlated exposure history, suggesting that the preservation of their sampling sites has been modified (supporting information Figure S1–S2).

To demonstrate the reliability of bedrock scarps for preserving earthquake and tectonic process, we present five new ^{36}Cl datasets from the Italian Apennines: three localities on the Campo Felice fault and two on the Roccapreturo fault (Figure 1). We focus on the central Italian Apennines because limestone fault scarps are common in the region and the faults are excellently exposed, well mapped, and easily accessible. There are 19 published ^{36}Cl sample sites in the region (Schlagenhauf et al., 2010; Benedetti et al., 2013; Tesson et al., 2016; Cowie et al., 2017, Figure 1). We also remodel data published by Benedetti et al. (2013) from a site on the Campo Felice fault and data published by Schlagenhauf (2009) from a site on the Roccapreturo fault, in order to directly compare with our new data on the same faults. Our sites were selected on the basis of extensive field reconnaissance, mapping, terrestrial laser scanning (TSL), and remote sensing surveys, in order to ensure that the slip preserved at the surface is the result of earthquake displacements and not affected by hillslope processes. We use a Markov chain Monte Carlo (MCMC) method to model the data at each site, which constrains the timing of slip rate changes to facilitate comparison of sample localities along strike. Our modelling approach incorporates uniform parameters related to early ^{36}Cl production at different sites from the same fault, using the timing of global climatic change as a constraint on how long the fault scarp has been preserved at each of our sampling locations. We show how our approach can be used to determine spatial and temporal variation in earthquake displacement on normal faults.

2 Geological background

2.1 Quaternary faulting in the central Apennines

GNSS measurements indicate that the central Italian Apennines is extending at a rate of 2.7 ± 0.2 mm yr^{-1} in a NE-SW direction, active since 2–3 Ma (D'Agostino et al., 2011; Roberts & Michetti, 2004, Figure 1). This extension has produced a series of NW-SE trending normal faults that host $>$M$_w$ 6 surface rupturing earthquakes, which are recorded in both the instrumental and historical records (Rovida et al., 2019; Walters et al., 2018). Average extension rate estimates for the region based on the offset of postglacial slopes by active faults since the Last Glacial Maximum (LGM) are 3.1 ± 0.7 mm yr^{-1} (Roberts & Michetti, 2004; Faure Walker et al., 2010), in agreement with GNSS rates. The Quaternary

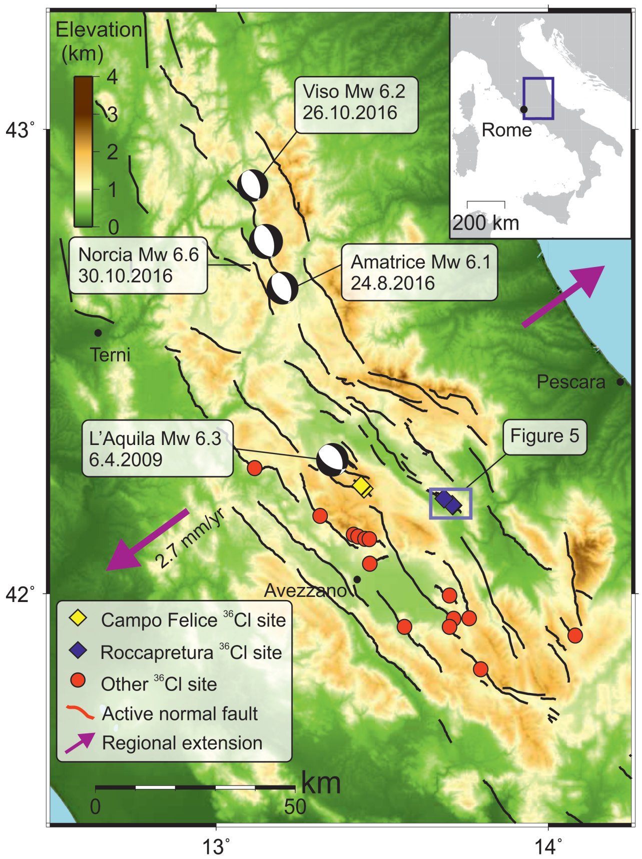

Figure 1. An overview of the central Italian Apennines showing fault scarp sample localities (yellow and blue diamonds). Additional site locations are from Palumbo et al. (2004); Schlagenhauf (2009); Schlagenhauf et al. (2011); Benedetti et al. (2013); Tesson et al. (2016); Cowie et al. (2017), earthquake moment tensors are from www.globalcmt.org, and the fault map is modified from Roberts and Michetti (2004). The regional extension direction indicated is based on D'Agostino et al. (2011). The DEM elevations are from 1 arcsecond (30 m) SRTM (Satellite Radar Topography Mission) data.

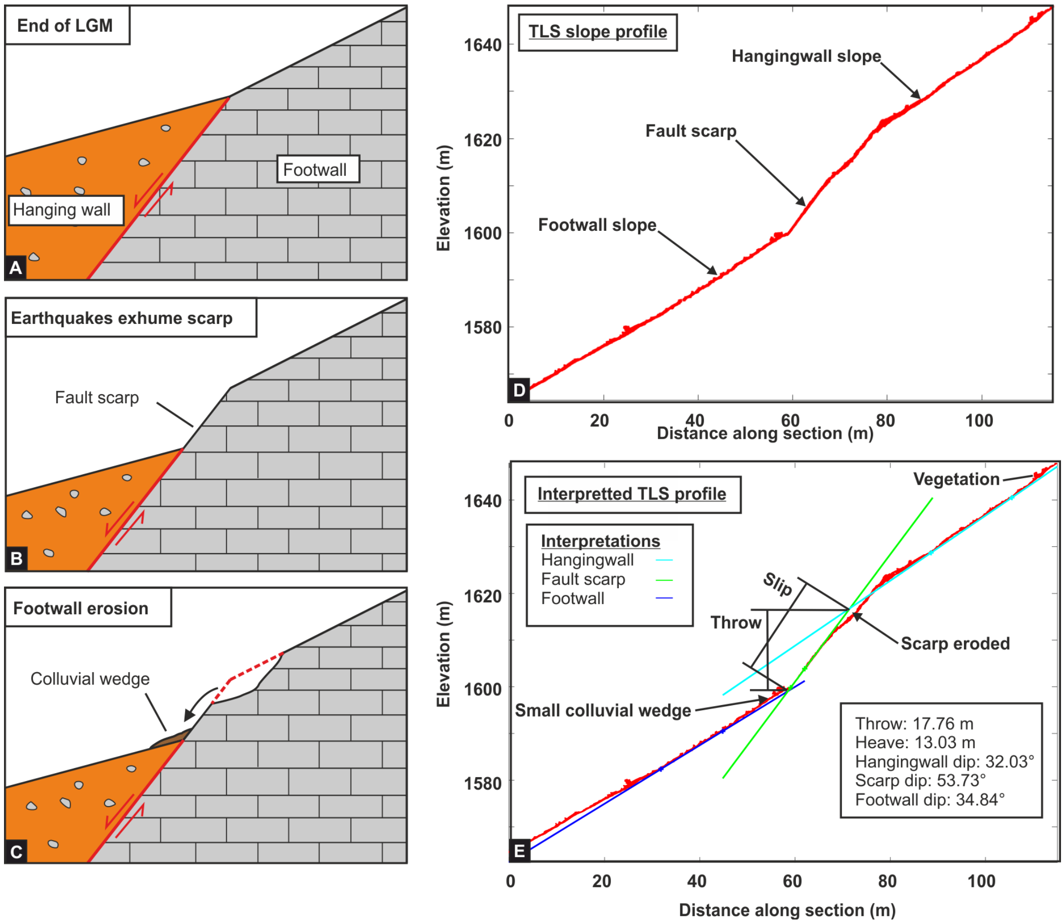

Figure 2. (A) Schematic model of fault scarp development when exhumation rate is slower than erosion rate, as was the case during the LGM in the Central Italian Apennines. (B) and (C) shows a schematic model of scarp evolution since the end of the LGM, when exhumation rate outpaces erosion rate. Panel (D) shows a typical fault-perpendicular profile, from the Campo Felice fault, through a point cloud generated from TLS data and (E) shows one profile interpretation. Samples are not collected from the eroded section of the fault scarp due to the uncertainty in the timing of erosion; only the planar lower section is sampled.

and geodetic extension rates are similar to average extension rates calculated using offset stratigraphy, indicating that the total extension rate across the region may have remained constant for the last 0.75 Ma (Roberts & Michetti, 2004). Time variable fault slip rates and spatio-temporal earthquake clusters have been inferred in the region based on models of ^{36}Cl cosmogenic data (Schlagenhauf et al., 2011; Benedetti et al., 2013; Cowie et al., 2017), and several spatially correlated (along-strike) sequences of large earthquakes have occurred in the modern record.

Planar limestone bedrock fault scarps have been preserved along normal faults since the demise of the LGM (10–20 ka) when the bedrock exhumation rate, normally as a result of fault displacement during earthquakes, exceeded the erosion rate of the fault scarp (Figure 2; e.g. Giraudi, 1995; Tucker et al., 2011; Bubeck et al., 2015; Giraudi et al., 2011). In the central Italian Apennines, fault scarps are observed in Mesozoic limestone, but scarps are poorly preserved where the faults pass into other lithologies, such as siliciclastic turbidite deposits. The preferential formation and preservation of fault scarps is due to the strong

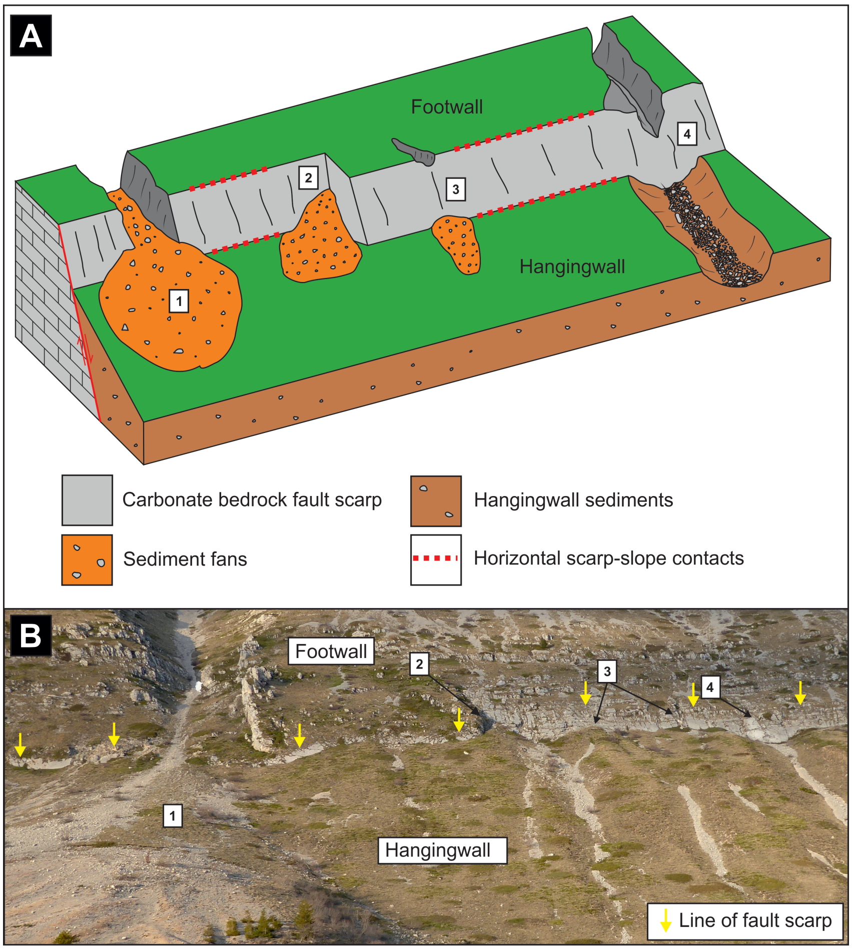

Figure 3. (A) Schematic diagram of slope processes that can lead to non-tectonic exhumation and burial of active limestone fault scarps. Labels 1-4 indicate areas of hangingwall erosion or deposition that are inappropriate sample locations. Ideal sites are located tens of metres away from areas affected by depositional and erosional slope processes, where the scarp-slope contacts are horizontal, after Bubeck et al. (2015). (B) The Campo Felice fault with features from (A) indicated. Photo taken from (42.2308°N, 13.4343°E), view northeast. The horizontal scale is approximately 320 m across image at the height of scarp.

erosional resistance of limestone fault surfaces, and is also well documented in Greece and western Turkey, which host lithologies similar to central Italy (Goldsworthy & Jackson, 2000; Akçar et al., 2012). Exhumation of bedrock fault scarps in the central Apennines is not always only due to fault slip in earthquakes. In many areas the footwall and hangingwall are subject to erosional and depositional processes that are currently active or have been active since the demise of the LGM. Removal or deposition of material on the hangingwall and footwall can contribute to the exhumation history of the scarp (Bubeck et al., 2015).

2.2 Fault geomorphology and site descriptions

We compare slip histories from the multiple sites on two faults: the Campo Felice and Roccapreturo faults (Figures 1 and 4). We sampled three new sites on the Campo Felice fault and two new sites on the Roccapreturo fault, and we also make use of previously published data from one site on each fault (Schlagenhauf, 2009; Benedetti et al., 2013). We describe how the sites were selected, the background literature, and geomorphology relating to both faults and all sample sites.

2.3 Sample locality selection

Sample localities are selected to minimise the impact of post-LGM depositional or aggradational processes acting to expose or bury the planar fault scarp (Figure 3). We follow the criteria set out by Bubeck et al. (2015) and Cowie et al. (2017) to identify suitable cosmogenic sampling sites that have a stable hangingwall and footwall slope. The new sites presented in this study fulfill the following five criteria: 1) the footwall and hangingwall slopes are intact, planar, and show no evidence of incision; 2) the hangingwall slope is free of post LGM sediments (typically associated with actively agrading alluvial fans, colluvial wedges, sloping footwall-hangingwall contacts, and the edge of major drainages); 3) the site is located away from fault relay zones (site RP2 is an exception); 4) the fault plane surface is well preserved; and 5) the contact between the free-face (fault plane) and the hangingwall slope is horizontal, ruling out along-strike mass movement.

We identify areas that conform to the first three of these criteria by investigating the contacts between the footwall, the fault scarp, and the hangingwall. Horizontal contacts at a consistent height over a distance of 10 meters or more indicate a lack of significant erosion or deposition since the demise of the LGM (Figure 3). The footwall slope should be smooth and uninterrupted by major drainages in the vicinity of the sample locality. We identify appropriate areas for sampling using a combination of satellite image analysis (Google Earth), interpretation of Terrestrial Laser Scanning (TLS)-derived point clouds, and fieldwork.

2.3.1 Campo Felice

The Campo Felice fault has a total length of ∼15 km. It is composed of two overlapping segments, an ∼6 km southern section striking on average 130° and an ∼8 km northern section with an average strike of 120°. The Campo Felice fault and the 8 by 3 km basin it bounds have been the focus of several studies (Giaccio et al., 2003; Giraudi et al., 2011; Giraudi, 2012; Benedetti et al., 2013; Wilkinson et al., 2015). The Campo Felice fault may have ruptured during an event in 1300 AD (∼ 720 ybp) based on paleoseismic data (Salvi et al., 2003), but this is not certain as the data are from a paleoseismic trench on a fault segment 5 km north of the main structure, which Salvi et al. (2003) propose is linked to the Campo Felice fault. Pantosti et al. (1996) undertook a paleoseismic study along the Ovindoli-Pezza fault, which is 5–6 km south east of the Campo Felice fault and could be a related structure (at depth). They suggest that earthquakes of M 6.5–7.0 occurred sometime between 700–1140 years ago, likely around 3900 years ago, and between 5300–7000 years ago on the Ovindoli-Pezza fault, and they estimated an average slip rate of 0.9–2.5 mm yr^{-1}. A terrestrial laser scanning (TLS) dataset was collected along the length of the Campo Felice fault by Wilkinson et al. (2015) to investigate the Quaternary activity and geomorphology, and we used these data paired with field reconnaissance to select appropriate sampling localities.

The footwall of the Campo Felice fault is characterized by a slope that is affected by the bedding of Upper Jurassic to Upper Cretaceous carbonates. The bedding dips sub-perpendicular to the slope dip, and sometimes forms prominent steps in the landscape, but the slope formed during glacial periods is distinct and dips towards the hangingwall basin. The footwall slope has active drainage channels and gullies between ∼1–100 m wide that feed debris fans and gullies in the hangingwall slope. Away from active drainage, the hangingwall and footwall slopes form smooth planar surfaces (Figure 2), similar to the idealised model shown in Figure 3a. The hangingwall slope is composed of an apron of well-cemented colluvium, typical of faults in the region. The bedrock fault scarp is generally well exposed and has a morphology typical of normal fault scarps in the region, and the trace of

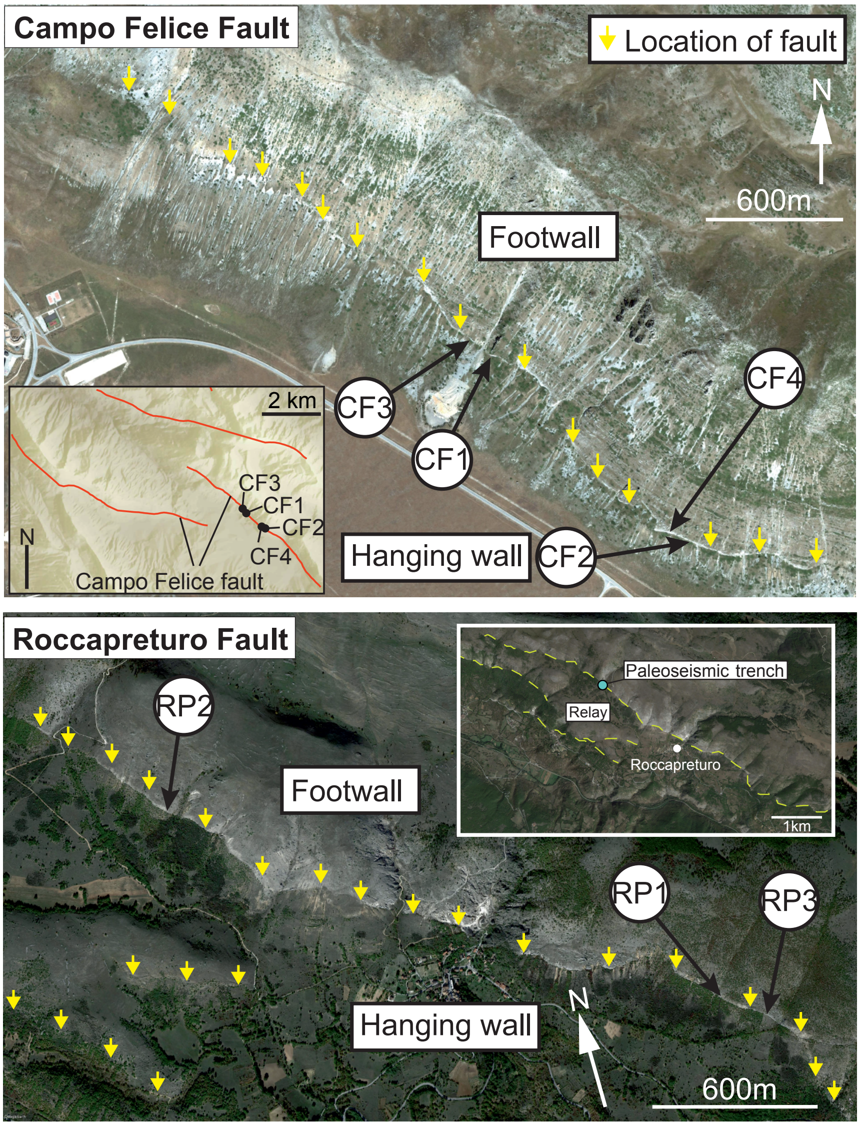

Figure 4. Location of sites used in this study, inset in the top panel shows the length of the Campo Felice fault. Campo Felice sites CF1, CF2, and CF3 were sampled during this study, and site CF4 was sampled and processed by (Benedetti et al., 2013). On the Roccapreturo fault (lower panel), sites RP1 and RP2 were sampled during this study, and site RP3 was sampled and processed by Schlagenhauf (2009). The inset panel shows the relay where two strands of the RP fault overlap. Imagery from Google Earth, 2018.

the scarp is located ∼60–200 m above the basin floor. Preservation of the planar fault scarp varies along strike, becoming more degraded near the fault tips. Further details of each site location and characterisation can be found in the supporting information, Figures S3–S8; Tables S1–S5.

There is one pre-existing ^{36}Cl sample site on the Campo Felice fault that was published by Benedetti et al. (2013), to which we will compare our new data and refer to as site CF4. The geomorphology at this sample site is stable and the scarp is well-preserved, as the site characteristics satisfy the criteria used for site selection outlined in our methodology. In this study we present results from three additional Campo Felice sites. Site CF1 was sampled in 2014 and Sites CF2 and CF3 were sampled in 2017. All sites are located on the southern segment of the fault along a ∼1 km long section (Figure 4). The distribution of sample sites was dictated by the geomorphology of the fault - we can only sample where the site criteria is acceptable and the bedrock scarp is well preserved.

2.3.2 Roccapreturo fault

The Roccapreturo fault is part of the Middle Aterno Valley Fault system (MAVF), which has a total length of 21 km (Galadini & Galli, 2000). The fault is composed of two segments: the southern segment is ∼8 km long, and the northern segment is ∼3 km long. A 1 km long relay zone separates the two segments, with the distance between the segments varying between 400–900 m (Figure 4 inset). The footwall is characterised by planar slopes incised by gullies up to ∼300 m wide. The hangingwall slope is composed of forested colluvium and the bedrock footwall has low density bushy vegetation.

A paleoseismological study of the Roccapreturo fault identified two events based on the offset of stratigraphic layers dated with radiocarbon techniques (Falcucci et al., 2015). The trenches of this study are located ∼400–500 m northwest along strike from site RP2 (Figure 4). The most recent event occurred between 1879–2009 BP and 3787–6055 BP and the penultimate event occurred between 3787–4055 BP and 7329–7499 BP (reported by Falcucci et al., 2015, as 2σ age ranges). Falcucci et al. (2015) used the offset of early Pleistocene breccias to calculate a slip rate on the Roccapreturo fault of between 0.23–0.34 mm yr^{-1}. The fault has been seismically inactive during the time period covered by the historical record (approximately the past 700 years, Galadini & Galli, 2000). Schlagenhauf (2009) sampled and modeled one ^{36}Cl site (herein referred to as RP3) on the Roccapreturo fault. They find that the scarp did not form in one event, but multiple events of unknown number and magnitude. They suggest that the most recent event occurred approximately 2.0–3.0 ka and that the entire scarp was exhumed between 2 ka and 6 ka BP. They report the total offset in the plane of the scarp as 10.2 m and have calculated the average slip rate during the period of exhumation to be 1.7 mm yr^{-1}. The geomorphology of this site does not meet the necessary site selection criteria described in this paper and Cowie et al. (2017), because it is located close to a gully that appears to have contributed to exhumation of the fault scarp (supporting information, Figure S9). We remodel their data using our approach in order to demonstrate the effect of enhanced erosion on cosmogenic data from bedrock fault scarps, comparing it with new data from localities with acceptable morphological characteristics.

We present data from two additional sites on the Roccapreturo fault, the first (RP1) located 180 m northwest along strike from site RP3 and the second (RP2) a further 2.5 km northwest along strike (Figure 4). Site RP2 is located within the relay zone of the two strands of the fault, and because some deformation may be shared between the overlapping parts of the fault we expect the resulting slip rates to be slower than the central portion of the main strand. However, the timing of slip rates changes (if there are changes) should coincide, as we assume large earthquakes rupture both strands of the fault. Details of site location and characterisation can be found in the supporting information, Figures S10–S13; Tables S1, S6–S7.

3 Methods

3.1 Sample collection and preparation

Limestone fault scarps are composed of fractured limestones with an increase in fracture density into the fault core where an indurated carbonate fault gouge is present. Where unaffected by erosion, the limestone scarps have planar surfaces with slickensides and striations commonly visible on the surface. We use these indicators to identify areas where the fault plane is well preserved, because erosion will destroy fault surface features. We avoid areas of fault plane that are intensely fractured or where the scarp is eroded, as well as areas with obvious secondary precipitation of calcite. We avoid fractures and secondary calcite in an attempt to sample fault rocks that are not contaminated with vadose carbonate cements that might contain cosmogenic chlorine produced in the atmosphere and circulated in groundwater (Dunai, 2010).

Sampling involves excavating a trench in the hangingwall against the fault scarp to a depth of 1–2 m. At most sites the density of the excavated colluvium is measured using a simplified version of the method outlined by Muller and Hamilton (1992), because colluvial density is a shielding parameter in the cosmogenic modelling. Discrete samples that are 15 cm wide x 5 cm high and 2.5 cm thick are cut from the exposed fault plane using a handheld angle grinder, along a line parallel to the slip vector on the fault (parallel to dip direction at all sites). Some samples are horizontally offset from the main vertical sample line to avoid eroded parts of the fault plane. Photos of each site including the location of the samples on the scarp are shown in the supplementary materials. We collect a 3D point cloud dataset using TLS at each sampling site and extract the geometry of the slip parallel profile of the slope using the Matlab® code *crossint* (Figure 2; Wilkinson et al., 2015; Cowie et al., 2017).

Sample preparation and measurement is undertaken following standard methods described by Cowie et al. (2017). Chemical sample preparation is conducted at the Leeds University Cosmogenic Isotope Laboratory and prepared samples are measured with the accelerator mass spectrometer (AMS) at the Scottish Universities Environmental Research Centre (SUERC). We report the ^{36}Cl concentration in atoms g^{-1}. Reported 1σ uncertainties are AMS analytical errors and include propagation of uncertainty based on procedural blanks and standard material measurements. Bulk rock chemistry is constrained by inductively coupled plasma optical emission spectrometry (ICP-OES) at the University of Leeds. Notably, sample aliquots for Ca weight % measurements must be diluted to $\sim$ 1 ppm Ca for accurate and repeatable measurements. A more detailed description of the sampling and laboratory processes, alongside full results tables enabling recalcuation of ^{36}Cl concentrations, can be found in the supporting information, Text S1.

3.2 Modelling of the data

Cowie et al. (2017) show that the relationship between ^{36}Cl and height on a fault scarp should approximately scale with the average fault slip rate, such that faster faults have a steeper slope in ^{36}Cl concentration versus height and slower faults have a shallow slope. The concentrations from two sites with a similar slip history (or rate) should approximately overlap, though this may not be precisely true if there is a difference in site geometries or target element abundance (e.g. calcium). ^{36}Cl concentrations from a bedrock scarp do not represent direct exposure ages, because a portion of the total ^{36}Cl in each sample is accumulated while the fault is partially buried in the shallow sub-surface. In order to model slip rate and the pattern of exhumation through time, we use a modified version of the Bayesian Markov chain Monte Carlo (MCMC) approach developed by Cowie et al. (2017) to explore the age-slip relationships that adequately explain the observed ^{36}Cl measurements within uncertainties (further described later in this section, the supplement, and available online, `github.com/lcgregory/SimpleSlips`). Bayesian statistical methods are widely applied in earth science and geochronology in order to incorporate prior information about a set of parameters and calculate the posterior distribution for a set of parameters given quantitative measurements, using a mathematical model (Bronk Ramsey, 2009; Montoya-Noguera & Wang, 2017). Bayesian inversions can also be transdimensional, meaning that the number of model parameters ('unknowns') for which we solve is allowed to vary, increasing or decreasing the complexity of the model depending on what is required by the data (Green, 1995; Sambridge et al., 2006; Bodin & Sambridge, 2009; Dettmer et al., 2010; Amey et al., 2019). We use a hyperparameter to vary the number of slip rate changes, which change in time and height, and can be added or removed (varying the number of model parameters), limited by a reversible jump algorithm that favors simple solutions (Sambridge et al., 2006). Bayesian techniques are often applied to deal with uncertainty associated with limited data (Bronk Ramsey, 2009; Montoya-Noguera & Wang, 2017; Amey et al., 2019). Several different Bayesian MCMC approaches have been developed for modelling cosmogenic data from fault scarps (Beck et al., 2018; Tesson & Benedetti, 2019; Tikhomirov et al., 2011). In this study, we prefer the modified version of the approach in Cowie et al. (2017) because our primary aim is to identify and compare first-order variations in fault slip rate. Whilst the code used here does not change some of the factors affecting production (attenuation depth and colluvial density), this code has fewer parameters than other available codes, and does not attempt to identify individual earthquakes, which fits within the limitations of our data.

The MCMC code relies on the modified version of the Matlab® code from Schlagenhauf et al. (2010) to forward model the ^{36}Cl concentration. The forward model simulates exhumation of a normal fault plane and calculates the resulting ^{36}Cl concentrations including corrections for parameters such as site geometry, sample composition, and cosmogenic particle flux. We employ a time varying cosmogenic particle flux derived for each site using the most recent cosmogenic calculator *CRONUS-2* described by Marrero et al. (2016). Further details on site-specific production rate scaling are included in the supporting information, Table S1. Previous studies use a constant value for colluvium density at each site (Cowie et al., 2017), and, given the poorly quantified uncertainties associated with determining mean colluviual density in the field, and the agreement of our measured values with average values previously determined, we also use a mean value of 1.5 g cm^{-3}.

At each sampling locality, the height of the preserved fault scarp is known (from TLS observations, Figure 2). There is a gap between the highest sample and the top of the scarp, because the top part has been subject to weathering processes for longer than the base and is poorly preserved. The exposure history of the unsampled portion of the scarp is modelled by assuming that the scarp has been preserved since the demise of the LGM. The MCMC algorithm explores a trans-dimensional parameter space, solving for both slip rate and the number and timing of changes in slip rate. A slip history is generated with parameters conditioned on the prior probability, to calculate a forward model of ^{36}Cl values for this slip history. The likelihood of the proposed slip history is calculated given the comparison between the modelled ^{36}Cl values relative to the measured data. The algorithm then varies one of the parameters used to define the slip history and runs the forward model again. The new slip history is accepted if it has a higher likelihood than the previous model or if the ratio of new/current likelihood is higher than a random number drawn from a uniform distribution between 0 and 1, otherwise the new model is rejected, as per the Metropolis Hastings algorithm (Metropolis et al., 1953; Hastings, 1970). We run this for 500k iterations.

The model parameters for which we solve to define a slip history are: 1) scarp age (SA, time of the first event that produced preserved fault scarp, with a 1σ normally distributed prior of 15$\pm$3 kyr), 2) elapsed time (ET, time since last earthquake, no prior unless something is known about the most recent earthquake), 3) timing of change points (timing of change in slip rate), 4) height on fault scarp of a change point and 5) a hyper-parameter, the number of change points. The slip rate between change points is kept constant. The actual number of parameters can vary between each iteration, dependent on how many change points are defined. In each iteration we make a small change to one of the parameters. Further details, including synthetic tests and examples from other faults, can be found in Cowie et al. (2017) and online. We use the flexible change point method of Cowie et al. (2017) rather than the

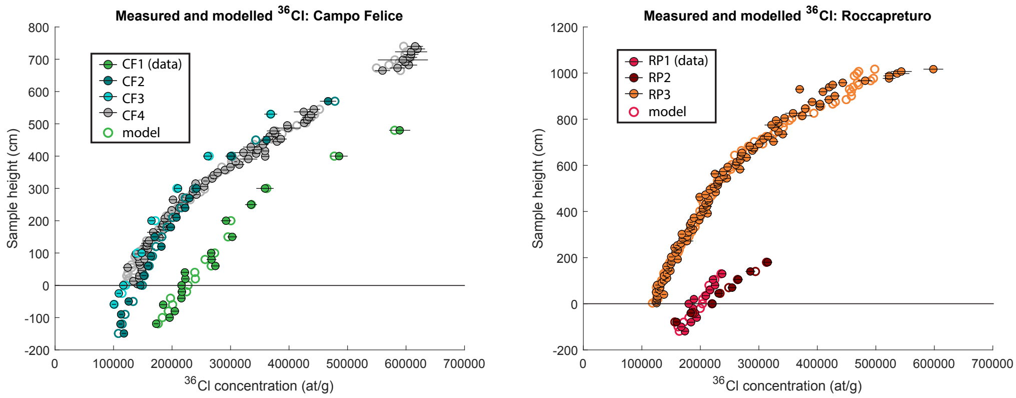

Figure 5. ^{36}Cl concentration versus sample height in the plane of slip. Each filled point represents a different sample, and each suite of coloured points represents data from one site as indicated. Open circles show the modelled ^{36}Cl from the MAP (maxium a posterior estimation). The colour scheme for each site is kept uniform in the figures that follow (CF4 is navy in following figures). Data from Campo Felice Site CF4 are from (Benedetti et al., 2013), and data from Roccapreturo Site RP3 are from Schlagenhauf (2009). Analytical 1σ uncertainties are plotted as black lines. These data are not corrected for calcium concentration, and some variation in ^{36}Cl between sites and noise in sample data is related to different production rates resulting from variable Ca.

fixed change point model (where the change point height up the fault scarp is fixed) because we have no additional data such as fault roughness to fix the height of the changes in slip rate up the scarp. The flexible change point model allows timing and number of changes in slip rate to vary between iterations, whilst the reversible-jump transdimensional algorithm naturally favours simpler models with fewer change points, potentially resolving the issue of over-fitting the data (Sambridge et al., 2006). The Bayesian MCMC algorithm results in a distribution of possible slip histories and their likelihood and misfit to the data. We then calculate the posterior probability by multipling the likelihood by the prior. We use a constant slip size of approximately 1 m to exhume the scarp incrementally in our modelling as we find that using a smaller constant slip size has little effect on the overall model results but does make the inversion process more computationally expensive (supporting information Figure S14). If we were attempting to model individual events then the choice of slip size would have to be further considered. We also run a suite of models at different constant slip rates, to determine whether a simple exposure history can adequately explain the data and fit the LGM hypothesis (supporting information, figures S15–S16).

4 Results

^{36}Cl data are plotted as cosmogenic isotope concentration versus sample height on Figure 5 for the Campo Felice and Roccapreturo faults. At each site, the ^{36}Cl concentration increases gradually with increasing height, due to higher parts of the scarp being exposed for longer. In general, data from different sites on each fault overlap, and the slope of ^{36}Cl concentration versus height is related to the slip rate on the fault, such that a steeper gradient indicates faster slip rates. The concentration at the height of zero is indicative of both the fault slip rate, and the time elapsed since the last earthquake, because the buried portion of the scarp has accumulated ^{36}Cl during the time since the last earthquake, such that a greater ^{36}Cl concentration at height 0 and in the trench can indicate a longer elapsed time. ^{36}Cl concentration profiles are similar for sites CF2, CF3, and CF4 whilst

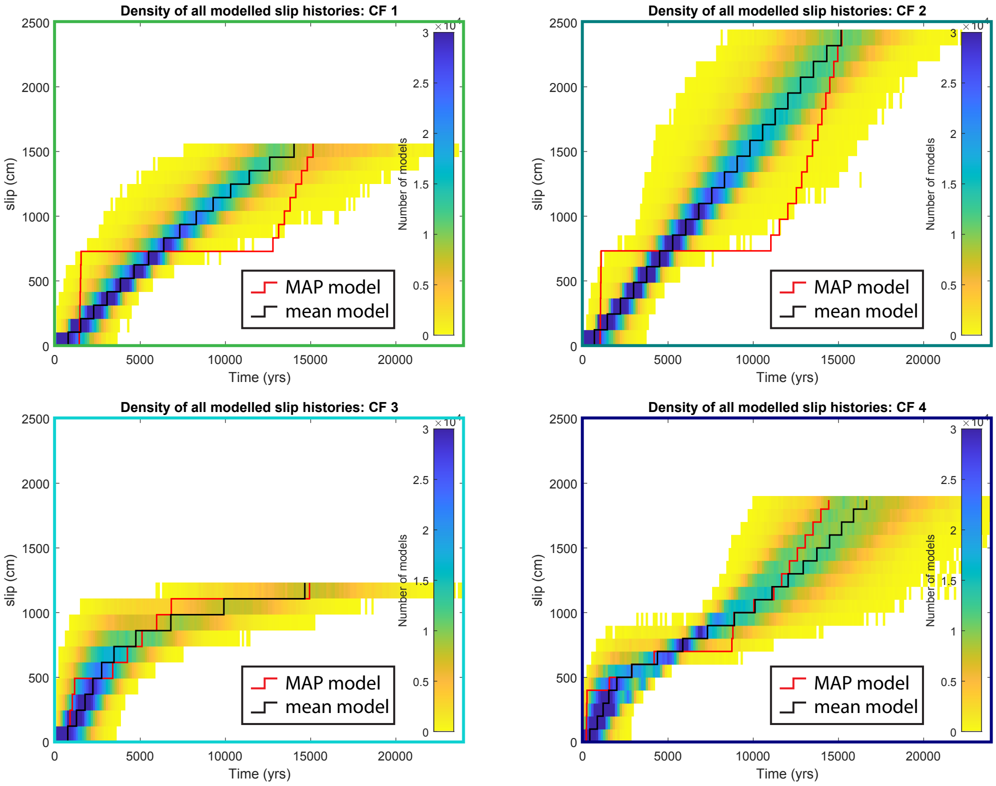

Figure 6. Modelling results from the Campo Felice fault ^{36}Cl data. Each sub-figure includes 500k iterations, minus the burn in of 50,000 iterations, as a 2D histogram showing the distribution of accepted slip histories in time-slip space. The distribution reflects the density of overlapping models, but does not capture the pattern of any individual slip history. The red line is the maximum a posteriori probability (MAP) estimation model, which is the maximum likelihood multiplied by the prior probability based on scarp age. The black line represents the mean model - which is the mean time for each slip step.

concentrations are greater at site CF1 for samples from the same height. All profiles show a change in gradient at ~3 m on the Campo Felice fault. On the Roccapreturo fault, site RP3 has lower ^{36}Cl concentrations for the same height than at sites RP1 and RP2, and has a steeper gradient at the base of the scarp compared to sites RP1 and RP2. The gradient at site RP3 gradually reduces with height. Sites RP1 and RP2 have similar ^{36}Cl concentrations, but with minor differences in gradient and the concentration at height 0. Site RP3 samples a section of preserved scarp that has an offset of 10.2 m, compared to sites RP1 and RP2 which have offsets of 7.2 m and 4.7 m respectively; this difference in heights is discussed in the context of the site geomorphology and strain partitioning in the discussion. Here we present the modelling results from each cosmogenic sampling site in the context of each fault and how the results can be compared between sites on the same fault.

4.1 Campo Felice fault

Each site was modelled with 500k iterations using the Bayesian inference MCMC code described in the methods section, with the site characteristics listed in Table S1, and modelling parameters in Table S8 (Cowie et al., 2017, `https://github.com/lcgregory/`

`SimpleSlips`). 2 dimensional histograms of all accepted exhumation models for each site with the burn in removed are shown in Figure 6. A burn-in of 50,000 iterations is removed from each set of results, because the initial models are affected by the starting parameter values. The histograms show the modelled distribution of time at which the fault surface was first exposed to the surface. The slip is modeled in approximately 1 meter increments in the slip direction and is binned into 200 year intervals in the histograms. In order to compare between sites, we plot the 95 percentile range of these same exhumation histories for all sites (Figure 7a). The models are poorly constrained above 7–10 m due to the lack of samples on the degraded part of the scarp, demonstrated by the increased variance between model results higher on the scarp. The ^{36}Cl concentration in each sample does reflect exposure of the fault surface at least 2 m above the sample due to being partially exposed to cosmic radiation whilst residing below the ground surface. As such, exposure of the un-sampled portion of the fault is somewhat constrained by the cosmogenic data at the top of the sampled portion, as well as by the independent prior in our modelling dictating that the top part of the scarp was preserved following the demise of the LGM (15 kyr with a 1σ standard deviation of 3 ka). However, the older portions of the slip models have more variability in exposure time, primarily due to the range in predicted ages for the demise of the LGM and preservation of the scarp (Figure 6). We rank the models by the posterior probability, which is the likelihood multiplied by the scarp age prior probability. We then select the top 10% most probable models to have the same distribution of the number of change points in the full distribution. The top 10% most probable models are used to calculate the average slip rate over time (Figure 7e), and the fit of CF1 models is shown in Figure 8a with the corresponding exposure histories. We also show the probability of events over time for the full model distribution in Figure 7c. Figure S17 shows the fit to the data of the full model distribution for each site on the Campo Felice fault. In general, the range of accepted models fit the data well (and all fit within the standard deviation of the data), though the top samples are poorly fit to the analytical errors by the least likely models.

For each site, we calculate the time-varying fault slip rate in mm yr^{-1} for the models that are the top 10% most probable (Figure 7e). Each model is a relatively simple time-slip vector, with a constant slip rate between the elapsed time, each change point, and the scarp age. The slip rate through time is the slope of each portion of each model at any given time. In order to average the variability across the accepted models, mean slip rates are calculated in 1 year increments (Figure 7e). Because one of the modeled parameters is the time elapsed since the last earthquake, each model has a period of time between the present day and the last proposed earthquake during which the incremental slip rate is zero. If another earthquake occurred today, the mean slip rate between the present day and what would then be the penultimate earthquake would change to accommodate the 'new' slip, but modeled slip rates previous to the penultimate event would remain the same. Therefore, the apparent drop to zero mm yr^{-1} in our slip rate calculations reflects the modeled elapsed time, and does not imply that the fault is inactive − an important consideration if time-varying fault slip rates are to be incorporated into earthquake hazard assessment. Because slip rate is calculated as mean of all of the models, we only show the rate up to 10 ka; older than 10 ka the slip rate is poorly constrained where the models 'end' at the scarp age and the mean is not representative.

In general, the modelling results show agreement in exposure histories between the sites (Figures 6 and 7a,c,e). Sites CF1 and CF3 are located within 150 m of each other, as are CF2 and CF4, and there is approximately 1 km between both sets of sites (Figure 4). There is a difference in scarp height between the group of northwestern sites (CF1 and CF3, average height 14 m) and the southeastern sites (CF2 and CF4, average height 21.5 m), but the height change does not lead to a significant difference in slip rate and the timing of change in slip rate during the past 0–7 ka, which is the best constrained time interval, because the ^{36}Cl concentrations at each site are all fit by an increase in slip rate during the same time interval. Models of sites CF1–CF3 have peak slip rates of 1.5–3 mm yr^{-1} between 500 and 2000 years, with a reduced slip rate of <1.5 mm yr^{-1} before approximately 3–4 ka

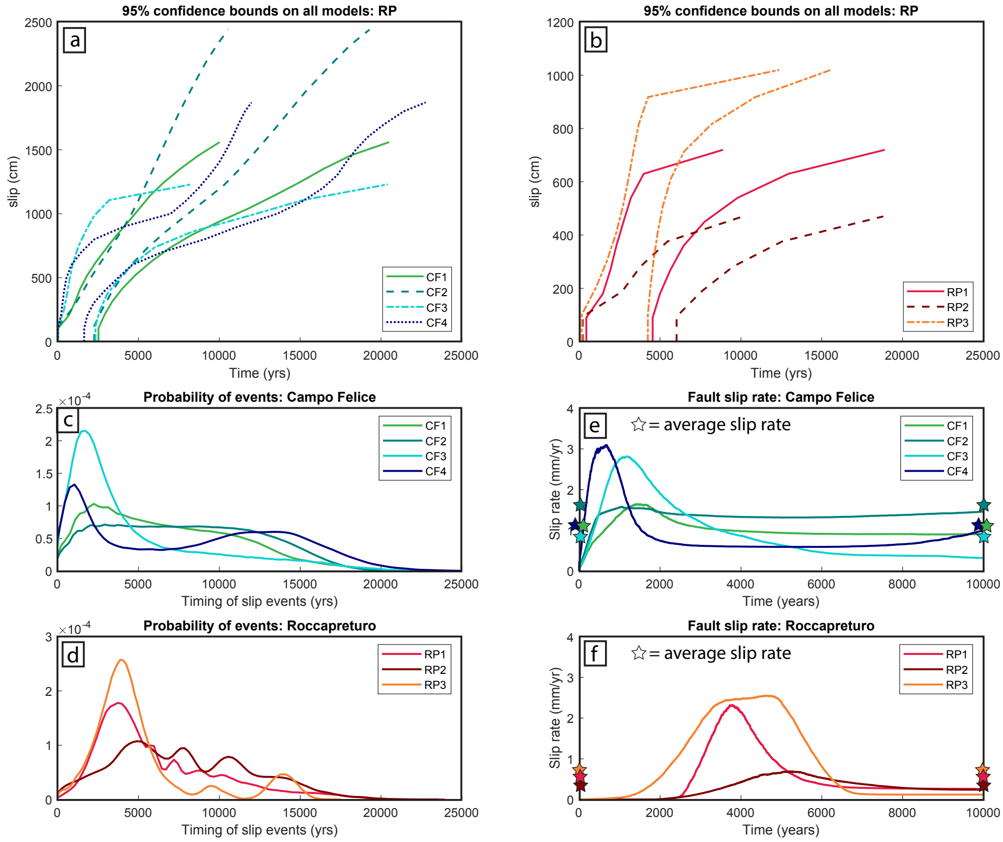

Figure 7. Summary of results from the Campo Felice and Roccapreturo faults. Panels (a) and (b) show the 95% confidence bounds on models from each site minus the burn in. Panels (c) and (d) show the probability distribution of slip events over time (for the full model results). Panels (e) and (f) show the average slip rate for the top 10% most probable models over time, in 1 year bins, and stars indicate the average slip rate calculated based on the median scarp age and scarp height.

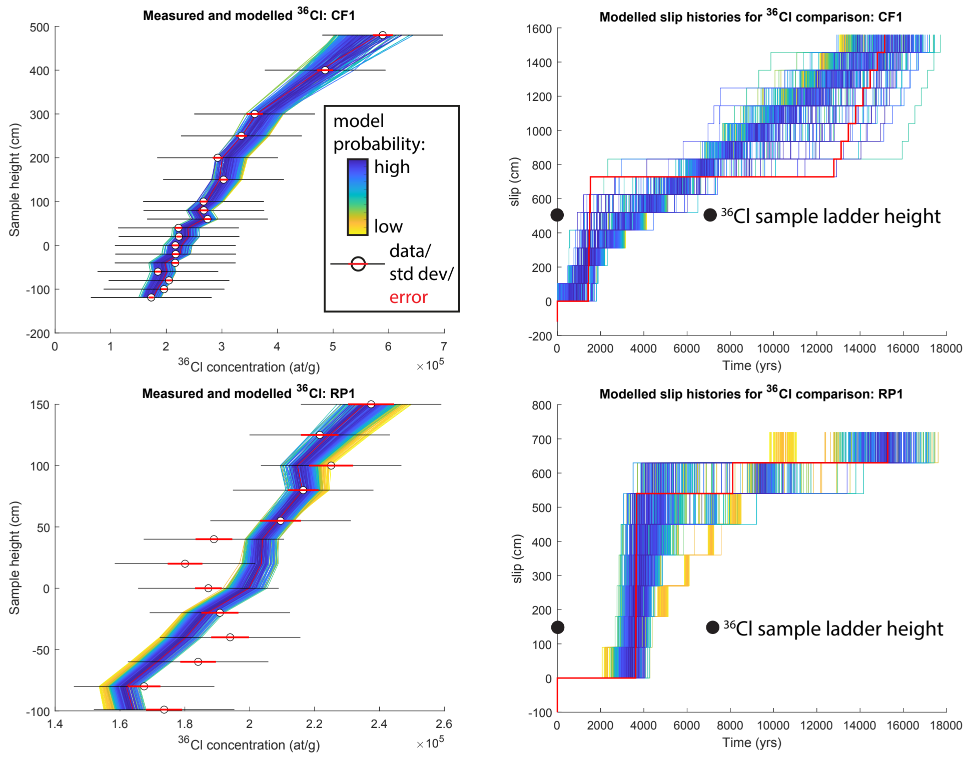

Figure 8. Figures (a) and (c) show the fit to data of models used to calculate average fault slip rates, for sites CF1 and RP1. The circles and error bars represent the ^{36}Cl measurements and the standard deviation of the data (used in the likelihood calculation); each colored line represents a model, with dark to light colours representing highest to lowest probability models, regulated by the scarp age probability and the number of change points. We present 400 models for each site ranging from the highest (dark blue) to lowest (yellow) probability at equal intervals (100) through the distribution. Figures (b) and (d) represent the corresponding model slip histories. The full distributions from the inversion for each site can be found in the Supplementary Materials.

(Figure 7e). Models of site C4 have a higher peak slip rate of just over 3 mm yr^{-1} occurring more recently than at sites 1–3 (around 0.5–1 ka), reflecting the lower ^{36}Cl concentration and steeper ^{36}Cl vs height at this site, requiring a faster slip rate more recently. Models of sites CF2 and CF4 have a second longer period of increased slip rate between the demise of the LGM and ∼8 ka, though this part of the exposure history is not well resolved, based on the spread of model results at the top of the scarp in Figure 6a-d. The results from all sites on the Campo Felice fault (Figure 7c) indicate that the fault was relatively active between 1–4 ka and relatively less active between 4–8 ka. The fault at sites CF1 and CF3 likely has less total slip in each event, compared to at sites CF2 and CF4, because the total scarp height is lower. Despite having less total slip, the timing of peak slip rate and rate change is correlated between all sites (Figure 7c,e).

4.2 Roccapreturo Fault

The modelling results from the Roccapreturo fault, including 2D histograms of slip versus time and mean slip rate through time, are shown in Figure 9, and the fits to the data of the 10% most probable models are shown in Figure 8. Site RP1 is located in the centre of the main fault strand, and RP2 is located on a relay between the main fault and a northern strand (Figure 4). Site RP3 was sampled by Schlagenhauf (2009) and is located near the southeastern tip of the main strand, on the edge of an active gulley (supporting information, Figure S9). The fault slip rates in Figure 7f are calculated for the 10% most probable models, and the probability of events over time is calculated for the full model distribution (Figure 7d). The general pattern of exhumation is characterised by relatively faster slip rate between 2–6 kyr, and slow to zero slip between 6 kyr and the demise of the LGM, and between the present to 2 kyr, which implies a long elapsed time. The maximum slip rates are 2.2, 0.7, and 2.5 mm yr^{-1} at sites RP1, RP2, and RP3 respectively. The difference in average slip rate between sites is primarily due to the difference in scarp height, as a larger scarp requires a faster rate of exhumation averaged over the time period. The decrease from fast to slow slip rate occurs at the same time at sites RP1 and RP2 (2.5–3 kyr), but RP3 has younger and more rapid peak in slip that lasts until 1.5–2 kyr, required by the much lower overall ^{36}Cl concentration and higher scarp height at the site (Figures 5 and 9). The modelling provides a good fit to the data at sites RP2 and RP3, but data just above the ground surface at RP1 are poorly fit (Figures 8 and S18). The pattern of these outlier data is not systematic, and suggests that there is additional noise that is not accounted for in some samples.

5 Discussion

Accurate fault slip rates derived from cosmogenic isotopes measured on bedrock fault scarps can contribute to our understanding of fault behavior over multiple earthquake cycles and should be considered when estimating seismic hazard (Benedetti et al., 2002; Schlagenhauf et al., 2010; Akçar et al., 2012; Cowie et al., 2017; Beck et al., 2018). However, until now it has not been demonstrated that results are consistent at different sites along strike on the same fault. Here we show that the timing of slip rate changes is similar at different sites along strike on the Campo Felice and Roccapreturo faults, but there are some differences in slip rate and total displacement between sites due to multiple factors. We discuss how the modelling parameters can be compared between sites, and highlight the assumptions and limitations of the ^{36}Cl method. We outline how results from sites with acceptable indicators of morphological preservation can be used to infer that both spatial (e.g. along strike on the fault) and temporal (changes in slip rate) variability is resolved on millennial timescales. We also compare our results with those from paleoseismic trenching on the same fault, which further supports the ability of cosmogenic isotopes measured on bedrock fault scarps to provide a reliable measure of fault activity.

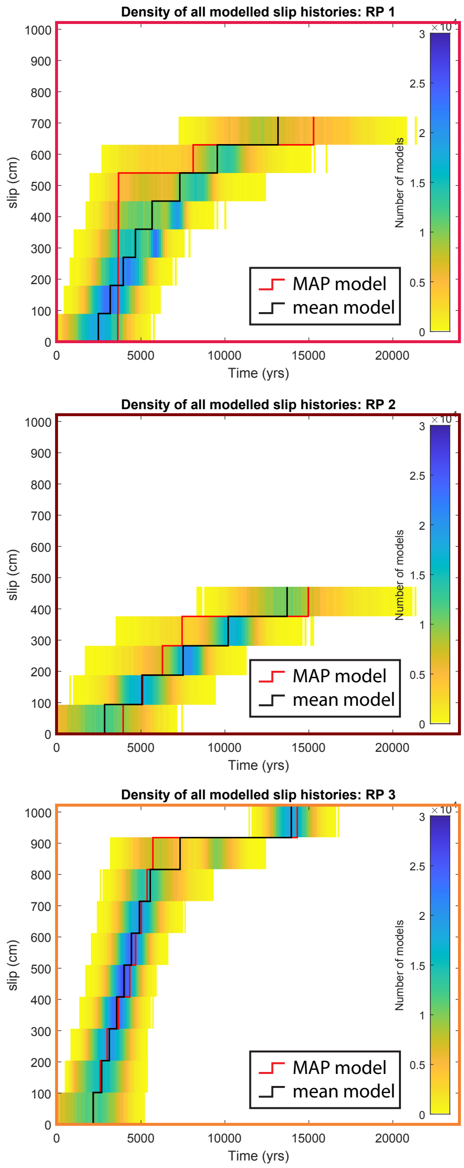

Figure 9. Modelling results from the Roccapreturo fault ^{36}Cl data. Each sub-figure includes 500k iterations, minus the burn in of 50,000 iterations, as a 2D histogram showing the distribution of accepted slip histories in time-slip space. The distribution reflects the density of overlapping models, but does not capture the pattern of any individual slip history. The red line is the maximum a posteriori probability (MAP) estimation model, which is the maximum likelihood multiplied by the prior probability based on scarp age. The black line represents the mean model - or the mean time for each slip step.

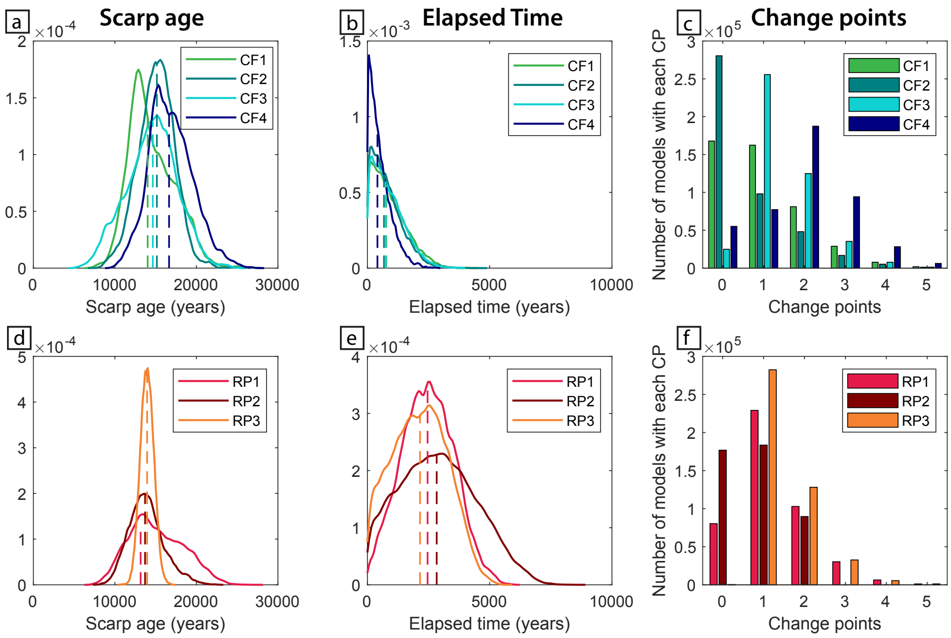

Figure 10. Posterior probability distribution functions for scarp age (a, c) and elapsed time parameters (b, e), for each fault with each site plotted as different coloured lines. The vertical dashed lines correspond to the median of each distribution. The number of change points (number of times the slip rate changes in each model) for each site is shown in c and f.

5.1 Along-strike comparison of fault activity

The magnitude of surface displacement in individual earthquakes can vary along-strike (Wesnousky, 2008; Rockwell & Klinger, 2013; P. O. Gold et al., 2013; Ando et al., 2017), and as the result the pattern of cumulative slip on a fault may be temporally synchronous but spatially variable in slip magnitude. Cosmogenic analyses on bedrock scarps provide constraints on both the time and cumulative displacement, so data from multiple sites can be used to isolate the spatial variation in slip along-strike over multiple earthquake cycles. Previous ^{36}Cl studies on bedrock normal scarps have concluded that significant temporal slip rate variations occur on thousand year time scales (Cowie et al., 2017; Schlagenhauf et al., 2010). Faults are demonstrated to have intervals of relatively fast slip rate or short earthquake recurrence intervals, interspersed with periods of relative quiescence. Changes in slip rate are probably linked to elastic interactions or strain partitioning processes that are larger in scale than a single fault (Cowie et al., 2012; Dolan et al., 2016) and, therefore, the timing of significant slip rate changes are likely to be temporally correlated along one fault.

We compare the posterior probabilities of the time of scarp preservation and the time since the most recent earthquake, the number of change points in each model run, and the average fault slip rate and timing of 'events' between the different sites on the same fault (Figure 7 and 10). One of the greatest uncertainties in modelling the cosmogenic data is the timing of preservation of the fault scarps, associated with the demise of the LGM and the transition from relatively fast to slow erosion of the scarp. We assign a wide Gaussian prior in our modelling to account for the uncertainty in how long it takes for fault activity to outpace erosion, and that this transition may be different for different faults. Figures 10a,d show the similarity in the posterior probability for scarp age at each site. We modelled the results from the Schlagenhauf et al. (2011) study using the same approach, and the scarp age posterior probabilities do not overlap (Figure S2), suggesting that morphological factors not associated with the LGM have affected the development of scarps at those sites.

Using the total displacement measured at each site and the median value for each scarp age posterior probability, we compute the Holocene average slip rate for each site (Table 1). The median represents the midpoint of the distributions, and is not affected as much by a small number of very large or small outliers as the mean value. We report the median and standard deviation of all sites based on the median of the combined posterior values for scarp age (divided by scarp height) of all sites. The median slip rate over the time since the demise of the LGM is 1.15 ± 0.36 mm yr^{-1} at Campo Felice based on all four sites and 0.42 ± 0.14 mm yr^{-1} at Roccapreturo, based on sites RP1 and RP2.

The elapsed time parameter only has a positivity prior value assigned in the modelling, because there are no paleoseismic trench sites within 2 km of our sites on the Campo Felice fault and there is no historical seismicity associated with either fault. The Campo Felice sites have a similar posterior probability distribution favouring an elapsed time of less than 800 years, with a non-normal distribution that is skewed towards younger values (median values range between 411–771 yrs, Figure 10b, Table 1). Paleoseismic data from trenches north and south of our site on adjacent fault strands indicate that the most recent surface rupturing event on the Campo Felice fault was 720 years (north segment) and between 700–1140 years (southeast segment - the Ovindoli-Pezza fault; Salvi et al., 2003; Pantosti et al., 1996). These results are in agreement with our estimated elapsed time, and they suggest that large earthquakes on the Campo Felice fault may involve multiple strands in the same earthquake, or sequences of events that occur over a relatively short time period, similar to several modern sequences in the region such as the 2016 central Italian sequence (Chiaraluce et al., 2017; Villani et al., 2018; Walters et al., 2018). Based on the interpreted surface displacements of 2–3 m, Pantosti et al. (1996) suggest that the causative event was a M 6.5–7.0, which is reasonable for a combined fault length of 35 km if all of the sampled segments were involved in one event. Pantosti et al. (1996) estimated that the average slip rate of the Campo Felice fault is 0.9–2.5 mm yr^{-1}, on the basis of multiple events occurring over the past 5300–7000 years, which also fits well with our long-term average fault slip rate (1.15 ± 0.36 mm yr^{-1}).

The Roccapreturo sites have a broad distribution of elapsed time values, with the median values at RP1 and RP2 in agreement (median = 2.6 ± 1.4 kyr, Figure 10e, Table 1), and a younger preferred value for site RP3 (median = 2.1 ± 1.1 kyr). These results agree with paleoseismic data that suggest the most recent event on the Roccapreturo fault was between 2–6 ka, with another large event occurring between 3.8–7.5 ka (Falcucci et al., 2015). These dates agree with the rapid slip rate between 2–7 ka at site RP2, which is located approximately 500 m from the paleoseismic trenches (Figures 4 and 7d,f). Whilst traditional paleoseismic data have been compared to ^{36}Cl slip histories in previous studies, these have either been on different fault strands at distances of >5 km (Tesson et al., 2016) or have suggested disparate results (Benedetti et al., 2003; Kokkalas et al., 2007). The agreement we find between the two techniques, which have been applied in such close proximity on the Roccapreturo fault, provides further evidence for the reliability of slip histories derived from modelling of ^{36}Cl on bedrock fault scarps, and the potential for these two techniques to be combined for more informed seismic hazard analysis.

There are many assumptions that must be taken into account when interpreting cosmogenic data from bedrock fault scarps. Because the top of the fault scarp is not well preserved and cannot be sampled, exposure histories older than ∼8–10 ka are poorly resolved and the modelling is reliant on estimates of how the scarp is preserved through the demise of the LGM (Figures 6 and 9 Schlagenhauf et al., 2011; Benedetti et al., 2013; Mechernich et al., 2018; Beck et al., 2018; Tesson & Benedetti, 2019). The trans-dimensional nature of the Bayesian inversion favors simple slip histories with the lowest number of changes in slip rate and we do not apply any weighting to the data other than the standard deviation of each

Table 1. Mean scarp age, elapsed time, and fault slip rates

Site name	Elapsed time (ET, yrs)	ET std[a] (yrs)	Scarp age (SA, yrs)	SA std (yrs)	Slip rate[b] (mm yr^{-1})	SR MAD (mm yr^{-1})
Campo Felice Fault						
CF1	771	684	14024	2841	1.11	0.21
CF2	678	619	15155	2238	1.61	0.27
CF3	476	634	14656	3139	0.84	0.23
CF4	411	445	16650	2688	1.12	0.18
CF median[c]	**631**	**620**	**15209**	**2909**	**1.15**	**0.36**
Roccapreturo Fault						
RP1	2461	1065	13162	2714	0.55	0.11
RP2	2891	1565	13856	2159	0.35	0.05
RP3	2140	1119	13960	825	0.73	0.04
RP median[c,d]	**2603**	**1355**	**13500**	**2460**	**0.42**	**0.14**

[a]Standard deviation.
[b]Holocene average slip rate calculated based on the height of the scarp divided by the scarp age pdf.
[c]Total median slip rate is calculated using the average scarp height divided by the pdf of scarp age at each site, and stacking the slip rate pdf.
[d]Calculated using only sites RP1 and RP2.

data set. The sampling bias is a challenge for calculating fault slip rates, because of the higher sample density at the base of the scarp. Consequently, the inversion favors simple slip histories that fit the data well in the bottom section of the scarp where there is a higher density of data, and that may fit less densely sampled data further up the scarp poorly. Models can fit the data with a more simple slip history by not fitting the top few data points as well as the data at the base of the scarp. If the oldest part of the exposure history can be better quantified, perhaps by incorporating more sophisticated geomorphological models and data constraining the timing of the LGM (e.g. Tucker et al., 2020), the entire slip history may be better determined.

At some sites no models fit the data to within the analytical uncertainties because they have outliers or noisy data that are not fit by any model. Applying site averaged calcium values at the two sites where we did not collect the data ourselves reduces the ability of models to fit the data because small variations in Ca concentration has a significant effect on the production rate of ^{36}Cl in each sample. One challenge in interpreting the output of MCMC Bayesian modelling is that, whilst there is a single best fit or most likely model, there are commonly hundreds or thousands of models that fit the data almost as well (Figure 8). After removing the burn-in, all of the models fit within the standard deviation of each data set, and can be incorporated when calculating average slip rates and making broad interpretations. Identifying higher frequency variations or individual slip events (earthquakes) is challenging because the data can be fit with a range of models, and is not possible using the data and modelling methods in this study. However, the first order variations in slip rate including pulses of rapid slip rate, which may represent temporal clustering of earthquakes, are consistent features in results from multiple sites along the same fault. The Bayesian MCMC approach with minimal parameters ensures that cosmogenic data are not overfit, and the result is an acceptable range of exposure histories, rather than a non-unique earthquake history.

Based on the results presented here and the large time and financial costs associated with sample processing and ^{36}Cl measurements, future studies may benefit from sampling multiple sites with discrete spaced samples rather than a continuous sample ladder at one sample site. The multi-site sampling approach also allows more information to be gained on along strike variability of slip rates. The geomorphology of each sample site should be carefully understood and documented to demonstrate the tectonic origin of bedrock fault scarps. Sampling at regular intervals on the fault scarp limits sampling bias and can reduce the complexity of interpreting modeled slip rates. While the prior that scarps are preserved only since the demise of the LGM is strongly supported in the Central Italian Apennines (Galadini et al., 2003; Tucker et al., 2011), application of the method to other regions will require equally robust evidence to define the scarp age prior distribution. Combining other data sources with the ^{36}Cl data, such as historical records and estimates from other dating techniques, helps to support results from cosmogenic data.

5.2 Temporal slip rate variability

Temporal slip rate variability is observed at all of the sites on the Campo Felice and Roccapreturo faults (Figure 10c,f). Both faults experience pulses of relatively fast slip rate (over thousands of years), peaking at 3 mm yr^{-1} at Campo Felice and 2 mm yr^{-1} at Roccapreturo, separated by intervals relative quiescence with slower average slip rate. Fault slip rate variability or discrepancies between geodetic, Quaternary, and geological slip rates is observed on many faults in various tectonic settings (Papanikolaou et al., 2005; Oskin et al., 2007; Faure Walker et al., 2010; Ferry et al., 2011; Dolan et al., 2016; Zinke et al., 2017), with several mechanisms invoked to explain the variability. Orogen-scale changes in erosion patterns or the kinematics, growth, and localisation of faulting may affect the comparison of geological rates ($> 10^5$) with geodetic and Quaternary rates (Hoth et al., 2006; Nicol et al., 2010). In the Italian Apennines, Cowie et al. (2017) suggest that time variable slip rates are primarily caused by large scale interaction across the whole fault network, in order to minimize the work done by faults. In this geodynamic model, different regions of faults are active at different times as a result of the change in gravitational potential energy acting on the uplifted footwall, inducing flexural bending of the normal fault footwall and time varying fault strength. Coulomb stress changes due to earthquakes are suggested to play a role in causing clustering of earthquakes and variable slip rates (Dolan et al., 2016; Wedmore et al., 2017). Dolan and Meade (2017) indicate that there is not yet a single mechanism that can explain this behavior across different faults, and suggest that it is caused by the complex interaction of processes that may be controlled by properties of a particular fault as well as the fault system as a whole. We observe peak slip rates at different times on the Campo Felice and Roccapreturo faults (Figure 10c,e), suggesting that fault activity migrates spatially over time between the two relatively close structures, possibly related to stress interaction (Figure 1).

In order to understand the mechanism behind slip rate variability on a single fault, it may also be informative to constrain the activity of faults in the rest of the network based on observations over multiple timescales. Probabilistic seismic hazard models currently use time averaged constant slip rates on faults (Valentini et al., 2017), and have limited temporal and spatial data coverage due to the sparsity of paleoseismic data sets (Dolan et al., 2016). What can be inferred from ^{36}Cl data on bedrock scarps is also limited in time, but we are able to capture 2 major changes in slip rate at some sites, helping to better understand the variability of earthquake recurrence on timescales that are important for understanding fundamental geological problems and seismic hazard. The method can be widely applied where scarps are preserved to reveal fault interaction on kilo-year timescales and to determine how several faults contribute to the large scale pattern of deformation. Slip rate variability may also be captured by quantifying slip rates using alternative methods that have different spatial and temporal coverage and resolution. Faure Walker et al. (2012) show that slip rates averaged over the Holocene (based on fault scarp heights) match the geodetic deformation rates, when averaged over large spatial scales (10^2 km). Cowie et al. (2013) suggest that the 10^4 year strain rates are representative of long-term geological rates based on the correlation between high strain and high topography, suggesting that faulting is driven by viscous flow on localised shear zones in the lower crust. ^{36}Cl derived slip histories have the potential to fill some of these spatial and temporal gaps and will help to elucidate the timing and mechanisms responsible for earthquake clustering and fault interaction.

5.3 Spatial fault complexity

The agreement between results from the Campo Felice Fault demonstrates that ^{36}Cl data from multiple sites spaced $\leq$1 km on one fault can be modeled successfully with similar slip histories. The larger fault scarp and a period additional slip between 7 ka and 15 ka only observed at the 2 southern most sites (sites CF2 and CF4, Figure 7c,e) may suggest that the fault does not always rupture continuously or uniformly along strike, which matches modern observations of faults in the region (Boncio et al., 2004; Walters et al., 2018; Villani et al., 2018). Sites CF1 and CF3 are closer to the overlap between the central and northwest Campo Felice fault strands (Figure 4), and it may be expected that total displacement is less at that location in each earthquake. Although Benedetti et al. (2013) determined an exposure history at site CF4 similar to our results, with 2 earthquakes at 1.1 ka, and events at 3.4, 4.2, 4.4, and 9.4 ka, their solution is non-unique, as there are many other exposure history that fit the data at CF4 equally well (Figure 6). The continuous ladder at CF4 leads to tighter constraint on parameters compared to sites CF1-CF3 (Figure 10). Models at site CF4 also include more change points than CF1-3 (Figure 10c), suggesting reliable more complex models (but not precise earthquake timings) can be generated from densely spaced data. This agrees with synthetic tests in Beck et al. (2018), which show that continuous sampling of the fault scarp does not necessarily resolve better constraints on absolute slip rates and the timing of change in slip rate compared to discrete sampling every 25–50 cm.

Modelled slip histories from sites on the Roccapreturo fault are not as similar as results from the Campo Felice fault. Site RP3, sampled by Schlagenhauf (2009), has a significantly larger fault scarp and a longer period of fast slip rate reaching 2 mm yr^{-1} from the present until 7–8 ka. The larger scarp at site RP3 is most likely a result of fast erosion of an unstable hangingwall on the edge of a major gully that incises the hangingwall and footwall of the fault (Figure 4). The fault scarp has been subject to active net erosive slope processes that likely removed material from the hangingwall slope exposing the fault surface in the gully, resulting in the higher scarp and faster slip rate than at other sites on the fault. The difference in timing of peak slip at site RP2 suggests that site RP1 experienced a more recent or larger slip event, implying that the fault does not always rupture continuously or that there is a variation in surface slip in a single event along the fault. We suggest that the slower average slip rate and shorter scarp height at site RP2 compared to site RP1 is because strain is partitioned between the end of the strand sampled (at RP2) and an overlapping fault strand located 1 km west and across strike (Figure 4). Between the two fault strands, there is a ramp in the topography that slopes down towards the southeast, and a step across each fault segment, perpendicular to fault strike, which is typical of a classic relay ramp morphology, where the length of the relay ramp is approximately 3 times the width (Fossen & Rotevatn, 2016, Figure 4).

Interaction between closely spaced fault segments can reduce the total displacement across individual faults due to strain partitioning, including at fault splays (McLeod et al., 2000; Cowie & Roberts, 2001; Manighetti et al., 2015). Our analyses at Roccapreturo suggests that over thousand year time scales the overlapping fault segments do not become completely inactive, but instead overlapping segments have slower average slip rates (or less slip per event) relative to the center of the main fault segment. Quaternary slip rate variation along strike is not typically observed at this scale and temporal resolution, demonstrating that ^{36}Cl provides a unique ability to investigate fault segment interaction and strain partitioning over millennial timescales. Due to the relatively young age of the normal fault network in the central Italian Apennines (2.3-3.3 Ma; Roberts et al., 2002) and low extension rates across the region (2.7 mm yr^{-1} D'Agostino et al., 2011), the fault system is immature, with a complex network of faults in the region that are highly interactive on relatively short timescales (including in earthquake sequences, e.g. Nixon et al., 2016). Individual faults in the central Apennines are still growing, and through the process of localisation, splays like the ones observed along the Roccapreturo fault may eventually become hard linked through to the surface and be capable of larger earthquakes and faster slip rates.

On the Campo Felice and Roccapreturo faults, we can observe the cumulative effect of the complexity of earthquake surface ruptures and resulting variation in displacement along strike. Some complexity arising during individual earthquakes may cumulatively cancel out over multiple earthquake cycles, if it is localised or random, and may contribute relatively insignificant noise to calculated slip rates. However if patches of high or low slip occur repeatedly in the same location on the fault, the displacement at any one site is not representative of either the fault rupture as a whole during that event, or that particular site over multiple earthquake cycles. We find that the variation in slip is consistent over multiple earthquakes cycles at some sites, such as site RP2 having lower slip than at RP1, and that sites CF2 and CF4 have higher slip than CF1 and CF3. By comparing ruptures from individual events with multiple offsets accumulated over longer timescales, it is possible to better understand along-strike variability (Brozzetti et al., 2019; Cinti et al., 2019).

6 Conclusions

We present ^{36}Cl cosmogenic isotope results and modelled exposure histories from 4 sites on the Campo Felice fault and 3 sites on the Roccapreturo fault. Unlike previous work, our modelling approach can be uniformly applied to all data in order to test whether they agree, without arbitrarily varying parameters related to the preservation of the fault scarps. Models from different sites on the same fault have the same long-term preservation age and elapsed time since the last earthquake, as well as similar long-term patterns of slip rate variability. The slip histories do not agree where samples are collected from unstable slopes, and there are parts of the faults that have slower average rates (likely caused by lower displacement in cumulative events), due to rupture complexity or strain partitioning between overlapping fault strands. Each fault experiences periods of time with much faster slip rates than the average Holocene rate, likely due to multiple earthquakes occurring over a few thousand years. The average slip rate for the Campo Felice fault is 1.15 ± 0.36 mm yr−1, and 0.42 ± 0.14 mm yr^{-1} on the Roccapreturo fault, with peak slip rates of 3 mm yr^{-1} and 2 mm yr^{-1} at each fault, respectively. The range of along-strike variability in slip rate means that one location may not represent the typical behaviour or hazard of an entire fault, and while sampling faults multiple times along strike is not always feasible, it can improve confidence in results by elucidating the range of slip rate and the timing of changes in slip rate.

Acknowledgments

This work was supported by the UK Natural Environment Research Council (NERC) through the NERC Centre for the Observation and Modelling of Earthquakes, Volcanoes and Tectonics (COMET), the Leeds-York NERC Doctoral Training Program NE/L0025274/1 (Goodall), Standard Grant NE/I024127/1 (Roberts/McCaffrey/Gregory/Phillips), NERC IRF NE/M019020/1 (Gregory), NE/S013911/1 (Amey) and the Royal Society CHG/R1/170038 (Amey). We are grateful to Greg Houseman, Tim Wright, and Richard Walters for providing their insight and discussion at all stages, and Tim Craig for discussion and writing the algorithm for calculating fault slip rate.

References

Akçar, N., Tikhomirov, D., Özkaymak, c., Ivy-Ochs, S., Alfimov, V., Sözbilir, H., ... Schlüchter, C. (2012). ^{36}Cl exposure dating of paleoearthquakes in the eastern mediterranean: First results from the western Anatolian extensional province, Manisa fault zone, Turkey [Journal Article]. *Geological Society of America Bulletin*, *124*(11-12), 1724-1735.

Amey, R., Hooper, A., & Morishita, Y. (2019). Going to any lengths: solving for fault size and fractal slip for the 2016 M_w 6.2 Central Tottori Earthquake, Japan, using a transdimensional inversion scheme. *Journal of Geophysical Research: Solid Earth*, *124*, 4001–4016.

Ando, R., Imanishi, K., Panayotopoulos, Y., & Kobayashi, T. (2017). Dynamic rupture propagation on geometrically complex fault with along-strike variation of fault maturity: insights from the 2014 Northern Nagano earthquake. *Earth, Planets and Space*, *69*, 130.

Armijo, R., Lyon-Caen, H., & Papanastassiou, D. (1992). East-west extension and Holocene normal-fault scarps in the Hellenic arc. *Geology*, *20*.

Beck, J., Wolfers, S., & Roberts, G. P. (2018). Bayesian earthquake dating and seismic hazard assessment using chlorine-36 measurements (bed v1). *Geoscientific Model Development*, *11*, 43834397.

Bendick, R., Bilham, R., Freymueller, J., Larson, K., & Yin, G. (2000). Geodetic evidence for a low slip rate in the Altyn Tagh fault system. *Nature*, *404*, 69–72.

Benedetti, L., Finkel, R., King, G., Armijo, R., Papanastassiou, D., Ryerson, F., ... Stavrakakis, G. (2003). Motion on the Kaparelli fault (Greece) prior to the 1981 earthquake sequence determined from ^{36}Cl cosmogenic dating. *Terra Nova*, *15*(2), 118–124.

Benedetti, L., Finkel, R., Papanastassiou, D., King, G., Armijo, R., Ryerson, F., ... Flerit, F. (2002). Post-glacial slip history of the Sparta fault (Greece) determined by ^{36}Cl cosmogenic dating: evidence for non-periodic earthquakes. *Geophysical Research Letters*, *29*(8).

Benedetti, L., Manighetti, I., Gaudemer, Y., Finkel, R., Malavieille, J., Pou, K., ... Keddadouche, K. (2013). Earthquake synchrony and clustering on Fucino faults (Central Italy) as revealed from in situ ^{36}Cl exposure dating [Journal Article]. *Journal of Geophysical Research: Solid Earth*, *118*(9), 4948-4974.

Bodin, T., & Sambridge, M. (2009). Seismic tomography with the reversible jump algorithm. *Geophysical Journal International*, *178*, 1411–1436. doi: doi:10.1111/j.1365-246X.2009.04226.x

Boncio, P., Giuseppina, L., Milana, G., & Rozzi, B. (2004). Seismogenesis in Central Apennines, Italy: an integrated analysis of minor earthquake sequences and structural data in the Amatrice-Campotosto area. *Annals of Geophysics*, *47*(6), 1723–1742.

Bronk Ramsey, C. (2009). Bayesian analysis of radiocarbon dates. *Radiocarbon*, *51*, 337–360.

Brozzetti, F., Boncio, P., Cirillo, D., Ferrarini, F., de Nardis, R., Testa, A., ... Lavecchia, G. (2019). High-resolution field mapping and analysis of the August-October 2016 coseismic surface faulting (Central Italy earthquakes): slip distribution, parametrization, and comparison with global earthquakes. *Tectonics*, *38*, 417–439.

Bubeck, A., Wilkinson, M., Roberts, G. P., Cowie, P., McCaffrey, K., Phillips, R., & Sammonds, P. (2015). The tectonic geomorphology of bedrock scarps on active normal faults in the Italian Apennines mapped using combined ground penetrating radar and terrestrial laser scanning. *Geomorphology*, *237*, 38–51.

Bull, J. M., Barnes, P. M., Lamarche, G., Sanderson, D. J., Cowie, P. A., Taylor, S. K., & Dix, J. K. (2006). High-resolution record of displacement accumulation on an active normal fault: implications for models of slip accumulation during repeated earthquakes. *Journal of Structural Geology*, *28*, 1146–1166.

Chiaraluce, L., Di Stefano, R., Tinti, E., Scognamiglio, L., Michele, M., Casarotti, E., ... Marzorati, S. (2017). The 2016 Central Italy seismic sequence: A first look at the mainshocks, aftershocks, and source models. *Seismological Research Letters*, *88*(3), 757–771.

Cinti, F. R., De Martini, P. M., Pantosti, D., Baize, S., Smedile, A., Villani, F., ... Brunori,

C. A. (2019). 22-kyr-long record of surface faulting along the source of the 30 October 2016 earthquake (Central Apennines, Italy), from integrated paleoseismic data sets. *Journal of Geophysical Research: Solid Earth*, *108*(5A), 2493–2520.

Cowie, P. A., Phillips, R., Roberts, G., McCaffrey, K., Zijerveld, L., Gregory, L., ... Wilkinson, M. (2017). Orogen-scale uplift in the central Italian Apennines drives episodic behaviour of earthquake faults. *Scientific reports*, *7*, 44858.

Cowie, P. A., & Roberts, G. P. (2001). Constraining slip rates and spacings for active normal faults. *Journal of Structural Geology*, *23*(12), 1901–1915.

Cowie, P. A., Roberts, G. P., Bull, J. M., & Visini, F. (2012). Relationships between fault geometry, slip rate variability and earthquake recurrence in extensional settings. *Geophysical Journal International*, *189*, 143–160.

Cowie, P. A., Scholz, C., Roberts, G. P., Walker, J. F., & Steer, P. (2013). Viscous roots of active seismogenic faults revealed by geologic slip rate variations. *Nature Geoscience*, *6*(12), 1036–1040.

Cowie, P. A., & Shipton, Z. K. (1998). Fault tip displacement gradients and process zone dimensions. *Journal of Structural Geology*, *20*(8), 983–997.

D'Agostino, N., Mantenuto, S., D'Anastasio, E., Giuliani, R., Mattone, M., Calcaterra, S., ... Bonci, L. (2011). Evidence for localized active extension in the central Apennines (Italy) from global positioning system observations. *Geology*, *39*(4), 291–294.

Dettmer, J., Dosso, S., & Holland, C. (2010). Trans-dimensional geoacoustic inversion. *Journal of the Acoustic Society of America*, *128*, 3393–3405.

Dolan, J. F., McAuliffe, L. J., Rhodes, E. J., McGill, S. F., & Zinke, R. (2016). Extreme multi-millennial slip rate variations on the Garlock fault, California: Strain super-cycles, potentially time-variable fault strength, and implications for system-level earthquake occurrence. *Earth and Planetary Science Letters*, *446*, 123–136.

Dolan, J. F., & Meade, B. J. (2017). A comparison of geodetic and geologic rates prior to large strike-slip earthquakes: A diversity of earthquake-cycle behaviors? *Geochemistry, Geophysics, Geosystems*, *18*(12), 4426–4436.

Dunai, T. J. (2010). *Cosmogenic nuclides: principles, concepts and applications in the earth surface sciences*. Cambridge University Press.

Falcucci, E., Gori, S., Moro, M., Fubelli, G., Saroli, M., Chiarabba, C., & Galadini, F. (2015). Deep reaching versus vertically restricted quaternary normal faults: Implications on seismic potential assessment in tectonically active regions: Lessons from the middle Aterno valley fault system, central Italy. *Tectonophysics*, *651*, 186–198.

Faure Walker, J., Roberts, G. P., Cowie, P., Papanikolaou, I., Michetti, A., Sammonds, P., ... Phillips, R. (2012). Relationship between topography, rates of extension and mantle dynamics in the actively-extending Italian Apennines. *Earth and Planetary Science Letters*, *325*, 76–84.

Faure Walker, J., Roberts, G. P., Sammonds, P., & Cowie, P. (2010). Comparison of earthquake strains over 10^2 and 10^4 year timescales: insights into variability in the seismic cycle in the central Apennines, Italy. *Journal of Geophysical Research*, *115*, B10418.

Ferry, M., Meghraoui, M., Abou Karaki, N., Al-Taj, M., & Khalil, L. (2011). Episodic behavior of the Jordan Valley section of the Dead Sea fault inferred from a 14-ka-long integrated catalog of large earthquakes. *Bulletin of the Seismological Society of America*, *101*(1), 39–67.

Fossen, H., & Rotevatn, A. (2016). Fault linkage and relay structures in extensional settingsa review. *Earth-Science Reviews*, *154*, 14–28.

Galadini, F., & Galli, P. (2000). Active tectonics in the central Apennines (Italy)–input data for seismic hazard assessment. *Natural Hazards*, *22*(3), 225–268.

Galadini, F., Messina, P., Giaccio, B., & Sposato, A. (2003). Early uplift history of the Abruzzi Apennines (central Italy): available geomorphological constraints. *Quaternary International*, *101*, 125–135.

Galli, P., Galadini, F., & Pantosti, D. (2008). Twenty years of paleoseismology in Italy. *Earth-Science Reviews*, *88*, 89–117.

Giaccio, B., Galadini, F., Sposato, A., Messina, P., Moro, M., Zreda, M., ... Todero, A. (2003). Image processing and roughness analysis of exposed bedrock fault planes as a tool for paleoseismological analysis: results from the Campo Felice fault (central Apennines, Italy). *Geomorphology*, *49*(3-4), 281–301.

Giraudi, C. (1995). Considerations on the significance of some post-glacial fault scarps in the Abruzzo Apennines (Central Italy. *Quaternary International*, *25*, 33–45.

Giraudi, C. (2012). The Campo Felice Late Pleistocene glaciation (Apennines, central Italy). *Journal of Quaternary Science*, *27*(4), 432–440.

Giraudi, C., Bodrato, G., Lucchi, M. R., Cipriani, N., Villa, I. M., Giaccio, B., & Zuppi, G. M. (2011). Middle and late Pleistocene glaciations in the Campo Felice Basin (central Apennines, Italy). *Quaternary Research*, *75*(1), 219–230.

Gold, P. O., Oskin, M. E., Elliott, A. J., Hinojosa-Corona, A., Taylor, M. H., Kreylos, O., & Cowgill, E. (2013). Coseismic slip variation assessed from terrestrial lidar scans of the El Mayor–Cucapah surface rupture. *Earth and Planetary Science Letters*, *366*, 151–162.

Gold, R. D., Briggs, R. W., Crone, A. J., & DuRoss, C. B. (2017). Refining fault slip rates using multiple displaced terrace risers–an example from the Honey Lake fault, NE California, USA. *Earth and Planetary Science Letters*, *477*, 134–146.

Gold, R. D., Cowgill, E., Arrowsmith, J. R., Gosse, J., Chen, X., & Wang, X.-F. (2009). Riser diachroneity, lateral erosion, and uncertainty in rates of strike-slip faulting: A case study from Tuzidun along the Altyn Tagh Fault, NW China. *Journal of Geophysical Research*, *114*, B04401.

Goldsworthy, M., & Jackson, J. (2000). Active normal fault evolution in Greece revealed by geomorphology and drainage patterns. *Journal of the Geological Society*, *157*(5), 967–981.

Gosse, J. C., & Phillips, F. M. (2001). Terrestrial in situ cosmogenic nuclides: theory and application. *Quaternary Science Reviews*, *20*, 1475–1560.

Green, P. (1995). Reversible jump Markov chain Monte Carlo computation and Bayesian model determination. *Biometrika*, *82*, 711–732. doi: https://doi.org/10.1093/biomet/82.4.711

Gregory, L., Thomas, A., Walker, R., Garland, R., Mac Niocaill, C., Fenton, C., ... West, A. (2014). Combined uranium series and ^{10}Be cosmogenic exposure dating of surface abandonment: a case study from the Ölgiy strike-slip fault in western Mongolia. *Quaternary Geochronology*, *24*, 27–43.

Hastings, W. (1970). Monte Carlo sampling methods using Markov chains and their applications. *Biometrika*, *57*(1), 97–109.

Hergert, T., & Heibach, O. (2010). Slip-rate variability and distributed deformation in the Marmara Sea fault system. *Nature Geoscience*, *3*, 132–135.

Hoth, S., Adam, J., Kukowski, N., & Oncken, O. (2006). Influence of erosion on the kinematics of bivergent orogens: Results from scaled sandbox simulations. In S. D. Willett, N. Hovius, M. T. Brandon, & D. M. Fisher (Eds.), *Tectonics, climate, and landscape evolution: Geological Society of America special paper 398, Penrose Conference Series* (pp. 201–225). Geological Society of America.

Hussain, E., Hooper, A., Wright, T. J., Walters, R. J., & Bekaert, D. P. (2016). Interseismic strain accumulation across the central North Anatolian fault from iteratively unwrapped insar measurements. *Journal of Geophysical Research: Solid Earth*, *121*(12), 9000–9019.

Kokkalas, S., Pavlides, S., Koukouvelas, I., Ganas, A., & Stamatopoulos, L. (2007). Paleoseismicity of the Kaparelli fault (eastern Corinth Gulf): evidence for earthquake recurrence and fault behavior. *BOLLETTINO-SOCIETA GEOLOGICA ITALIANA*, *126*(2), 387.

Manighetti, I., Caulet, C., Barros, L., Perrin, C., Cappa, F., & Gaudemer, Y. (2015). Generic along-strike segmentation of Afar normal faults, East africa: Implications on fault growth and stress heterogeneity on seismogenic fault planes. *Geochemistry, Geophysics, Geosystems*, *16*(2), 443–467.

Marrero, S. M., Phillips, F. M., Borchers, B., Lifton, N., Aumer, R., & Balco, G. (2016). Cosmogenic nuclide systematics and the cronuscalc program. *Quaternary Geochronology*, *31*, 160–187.

McLeod, A. E., Dawers, N. H., & Underhill, J. R. (2000). The propagation and linkage of normal faults: insights from the strathspey–brent–statfjord fault array, northern north sea. *Basin Research*, *12*(3-4), 263–284.

Mechernich, S., Schneiderwind, S., Mason, J., Papanikolaou, I. D., Deligiannakis, G., Pallikarakis, A., . . . Reicherter, K. (2018). The seismic history of the pisia fault (eastern corinth rift, greece) from fault plane weathering features and cosmogenic 36cl dating. *Journal of Geophysical Research: Solid Earth*.

Metropolis, N., Rosenbluth, A. W., Rosenbluth, M. N., & Teller, A. H. (1953). Equation of state calculations by fast computing machines. *The Journal of Chemical Physics*, *21*, 1087–1092.

Montoya-Noguera, S., & Wang, Y. (2017). Bayesian identification of multiple seismic change points and varying seismic rates caused by induced seismicity. *Geophysical Research Letters*, *44*, 3509–3516. doi: 10.1002/2016GL072266

Mueller, K. (2017). Variation in slip rates on active faults: Natural growth or stress transients? *Geology*, *45*(3), 287–288.

Muller, R. N., & Hamilton, M. E. (1992). A simple, effective method for determining the bulk density of stony soils. *Communications in soil science and plant analysis*, *23*(3-4), 313–319.

Nicol, A., J, W. J., Seebeck, H., & Berryman, K. R. (2010). Normal fault interactions, paleoearthquakes and growth in an active rift. *Journal of Structural Geology*, *32*, 1101–1113.

Nixon, C. W., McNeill, L. C., Bull, J. M., Bell, R. E., Gawthorpe, R. L., Henstock, T. J., . . . Kranis, H. (2016). Rapid spatiotemporal variations in rift structure during development of the Corinth Rift, central Greece. *Tectonics*, *35*, 1225–1248.

Oskin, M., Perg, L., Blumentritt, D., Mukhopadhyay, S., & Iriondo, A. (2007). Slip rate of the Calico fault: Implications for geologic versus geodetic rate discrepancy in the Eastern California Shear Zone. *Journal of Geophysical Research Solid Earth*, *112*(B7), B03402.

Palumbo, L., Benedetti, L., Bourles, D., Cinque, A., & Finkel, R. (2004). Slip history of the Magnola fault (Apennines, Central Italy) from ^{36}Cl surface exposure dating: evidence for strong earthquakes over the holocene [Journal Article]. *Earth and Planetary Science Letters*, *225*(1), 163-176.

Pantosti, D., D'Addezio, G., & Cinti, F. R. (1996). Paleoseismicity of the Ovindoli-Pezza fault, central Apennines, Italy: A histroy including a large, previously unrecorded earthquake in the Middle Ages (860–1300 A.D.). *Journal of Geophysical Research*, *101*(B3), 5937–5959.

Papanikolaou, I. D., Roberts, G. P., & Michetti, A. M. (2005). Fault scarps and deformation rates in Lazio–Abruzzo, Central Italy: Comparison between geological fault slip-rate and gps data. *Tectonophysics*, *408*(1-4), 147–176.

Peacock, D. C. P., & Sanderson, D. J. (1991). Displacements, segment linkage and relay ramps in normal fault zones. *Journal of Structural Geology*, *13*(6), 721–733.

Phillips, R. J., Parrish, R. R., & Searle, M. P. (2004). Age constraints on ductile deformation and long-term slip rates along the Karakoram fault zone, ladakh. *Earth and Planetary Science Letters*, *226*(3-4), 305–319.

Roberts, G. P., & Michetti, A. M. (2004). Spatial and temporal variations in growth rates along active normal fault systems: an example from the Lazio Abruzzo Apennines, central Italy. *Journal of Structural Geology*, *26*(2), 339–376.

Roberts, G. P., Michetti, A. M., Cowie, P., Morewood, N. C., & Papanikolaou, I. (2002). Fault slip-rate variations during crustal-scale strain localisation, central Italy. *Geophysical Research Letters*, *29*(8), 9–1.

Rockwell, T. K., & Klinger, Y. (2013). Surface rupture and slip distribution of the 1940 Imperial Valley earthquake, Imperial fault, southern California: implications for rupture segmentation and dynamics. *Bulletin of the Seismological Society of America*, *103*(2A), 629–640.

Rovida, A. N., Locati, M., Camassi, R. D., Lolli, B., & Gasperini, P. (2019). *Italian parametric earthquake catalogue (CPTI15, version 2.0.* Istituto Nazionale di Geofisica e Vulcanologia (INGV). doi: https://doi.org/10.13127/CPTI/CPTI15.2

Salvi, S., Cinti, F., Colini, L., D'addezio, G., Doumaz, F., & Pettinelli, E. (2003). Investigation of the active celano–l'aquila fault system, abruzzi (central apennines, italy) with combined ground-penetrating radar and palaeoseismic trenching. *Geophysical Journal International*, *155*(3), 805–818.

Sambridge, M., Gallagher, K., Jackson, A., & Rickwood, P. (2006). Trans-dimensional inverse problems, model comparison and the evidence. *Geophysical Journal International*, *167*(2), 528–542. doi: 10.1111/j.1365-246X.2006.03155.x

Schlagenhauf, A. (2009). *Identification des forts séismes passés sur les failles normales actives de la région lazio-abruzzo (italie centrale) par'datations cosmogéniques'(^{36}Cl) de leurs escarpements* (Unpublished doctoral dissertation). Grenoble 1.

Schlagenhauf, A., Gaudemer, Y., Benedetti, L., Manighetti, I., Palumbo, L., Schimmelpfennig, I., … Pou, K. (2010). Using in situ chlorine-36 cosmonuclide to recover past earthquake histories on limestone normal fault scarps: a reappraisal of methodology and interpretations. *Geophysical Journal International*, *182*(1), 36. Retrieved from +http://dx.doi.org/10.1111/j.1365-246X.2010.04622.x doi: 10.1111/j.1365-246X.2010.04622.x

Schlagenhauf, A., Manighetti, I., Benedetti, L., Gaudemer, Y., Finkel, R., Malavieille, J., & Pou, K. (2011). Earthquake supercycles in central Italy, inferred from ^{36}Cl exposure dating [Journal Article]. *Earth and Planetary Science Letters*, *307*(3), 487-500.

Schmidt, S., Hetzel, R., Kuhlmann, J., Mingorance, F., & Ramos, V. A. (2011). A note of caution on the use of boulders for exposure dating of depositional surfaces. *Earth and Planetary Science Letters*, *302*, 60–70.

Searle, M., Elliott, J., Phillips, R., & Chung, S.-L. (2011). Crustal-lithospheric structure and continental extrusion of Tibet. *Journal of the Geological Society, London*, *168*, 633–672.

Tesson, J., & Benedetti, L. (2019). Seismic history from in situ 36cl cosmogenic nuclide data on limestone fault scarps using bayesian reversible jump markov chain monte carlo. *Quaternary Geochronology*.

Tesson, J., Pace, B., Benedetti, L., Visini, F., Delli Rocioli, M., Arnold, M., … Keddadouche, K. (2016). Seismic slip history of the Pizzalto fault (central Apennines, Italy) using in situ-produced 36cl cosmic ray exposure dating and rare earth element concentrations. *Journal of Geophysical Research: Solid Earth*, *121*(3), 1983–2003.

Tikhomirov, D., Amiri, N. M., Ivy-Ochs, S., Alfimov, V., Vockenhuber, C., & Akçar, N. (2011). Fault scarp dating tool - a MATLAB code for fault scarp dating using in-situ chlorine-36 supplemented with datasets of Yavansu and Kalafat faults. *Journal of Geophysical Research: Earth Surface*, *116*(F1).

Tucker, G. E., Hobley, D. E. J., McCoy, S. W., & Struble, W. T. (2020). Modeling the shape and evolution of normal-fault facets. *Journal of Geophysical Research: Earth Surface*, *125*(e2019JF005305).

Tucker, G. E., McCoy, S. W., Whittaker, A. C., Roberts, G. P., Lancaster, S. T., & Phillips, R. (2011). Geomorphic significance of postglacial bedrock scarps on normal-fault footwalls. *Journal of Geophysical Research: Earth Surface*, *116*(F1).

Valentini, A., Visini, F., & Pace, B. (2017). Integrating faults and past earthquakes into a probabilistic seismic hazard model for peninsular Italy. *Natural Hazards Earth System Sciences*.

Villani, F., Civico, R., Pucci, S., Pizzimenti, L., Nappi, R., Marco De Martini, P., & th Open EMERGEO Working Group. (2018). A database of the coseismic effects following the 30 October 2016 Norcia earthquake in Central Italy. *Scientific Data*, *5*(180049).

Walters, R., Elliott, J., & Parsons, B. (2013). Rapid strain accumulation on the Ashkabad fault (Turkmenistan) from atmosphere-corrected InSAR. *Journal of Geophysical*

Research: Solid Earth, *118*, 3674–3690.

Walters, R., Gregory, L., Wedmore, L., Craig, T., McCaffrey, K., Wilkinson, M., ... others (2018). Dual control of fault intersections on stop-start rupture in the 2016 Central Italy seismic sequence. *Earth and Planetary Science Letters*, *500*, 1–14.

Wang, Y., Sieh, K., Aung, T., Min, S., Khaing, S. N., & Tun, S. T. (2011). Earthquakes and slip rate of the southern Sagaing fault: insights from an offset ancient fort wall, lower Burma (Myanmar). *Geophysical Journal International*, *185*(1), 49–64.

Wedmore, L., Walker, J. F., Roberts, G. P., Sammonds, P., McCaffrey, K., & Cowie, P. (2017). A 667 year record of coseismic and interseismic coulomb stress changes in central Italy reveals the role of fault interaction in controlling irregular earthquake recurrence intervals. *Journal of Geophysical Research: Solid Earth*, *122*(7), 5691–5711.

Wesnousky, S. G. (2008). Displacement and geometrical characteristics of earthquake surface ruptures: issues and implications for seismic-hazard analysis and the process of earthquake rupture. *Bulletin of the Seismological Society of America*, *98*(4), 1609–1632.

Wilkinson, M., Roberts, G. P., McCaffrey, K., Cowie, P. A., Walker, J. P. F., Papanikolaou, I., ... others (2015). Slip distributions on active normal faults measured from LiDAR and field mapping of geomorphic offsets: an example from L'Aquila, Italy, and implications for modelling seismic moment release. *Geomorphology*, *237*, 130–141.

Zechar, J. D., & Frankel, K. L. (2009). Incorporating and reporting uncertainties in fault slip rates. *Journal of Geophysical Research*, *114*, B12407.

Zinke, R., Dolan, J. F., Rhodes, E. J., Van Dissen, R., & McGuire, C. P. (2017). Highly variable latest Pleistocene-Holocene incremental slip rates on the Awatere fault at Saxton River, South Island, New Zealand, revealed by lidar mapping and luminescence dating. *Geophysical Research Letters*, *44*(22).